AD NUMBER

AD342207

CLASSIFICATION CHANGES

TO: unclassified

FROM: secret

LIMITATION CHANGES

TO:

Approved for public release, distribution unlimited

FROM:

Notice: Only military offices may request from DDC. Not releasable to foreign nationals.

AUTHORITY

DTRA ltr., 24 Jun 98; DTRA ltr., 24 Jun 98

WT-9003
Copy No. 13

GENERAL REPORT ON WEAPONS TESTS

LONG-DISTANCE BLAST PREDICTIONS, MICROBAROMETRIC MEASUREMENTS, AND UPPER-ATMOSPHERE METEOROLOGICAL OBSERVATIONS FOR OPERATIONS UPSHOT-KNOTHOLE, CASTLE, AND TEAPOT

Issuance Date: September 20, 1957

RESTRICTED DATA

This document contains restricted data as defined in the Atomic Energy Act of 1954. Its transmittal or the disclosure of its contents in any manner to an unauthorized person is prohibited.

SANDIA CORPORATION · ALBUQUERQUE, NEW MEXICO

SECRET

This report supersedes WT-9003(Prelim.), Series A. Holders of WT-9003(Prelim.) should destroy copies in accordance with existing security regulations. Destruction certificates should be forwarded to the Sandia Corporation, Albuquerque, N. Mex.

If WT-9003, Series B, is no longer needed, return it to
AEC Technical Information Service Extension
P. O. Box 401
Oak Ridge, Tennessee

WT-9003
This document consists of 90 pages
No. 55 of 180 copies, Series B
215

LONG-DISTANCE BLAST PREDICTIONS, MICROBAROMETRIC MEASUREMENTS, AND UPPER-ATMOSPHERE METEOROLOGICAL OBSERVATIONS FOR OPERATIONS UPSHOT-KNOTHOLE, CASTLE, AND TEAPOT

By

E. F. Cox

and

J. W. Reed

Sandia Corporation
Albuquerque, New Mexico
October 1956

RESTRICTED DATA

This document contains restricted data as defined in the Atomic Energy Act of 1954. Its transmittal or the disclosure of its contents in any manner to an unauthorized person is prohibited.

ABSTRACT

A blast prediction and microbarograph observation program was operated by Sandia Corporation during Operations Upshot-Knothole, Castle, and Teapot. Refined methods for blast prediction have been derived which appear to predetermine adequately the possibility of blast damages occurring outside the Nevada Test Site during test operations. In addition, sound recordings have been used for inverted geophysical seismic exploration of winds and temperatures in the ozonosphere, 30-60 km above the earth.

CONTENTS

ILLUSTRATIONS

ILLUSTRATIONS (cont)

ILLUSTRATIONS (cont)

TABLES

CHAPTER 3 PREDICTING SIGNAL PROPAGATION

CHAPTER 4 VERIFICATION OF PREDICTIONS

CHAPTER 5 UPPER ATMOSPHERE (OZONOSPHERE, IONOSPHERE) SIGNALS

CHAPTER 1

THE PROBLEM OF LONG-DISTANCE BLAST EFFECTS AT THE NEVADA TEST SITE

During Operation Ranger in 1951 at the Nevada Test Site (NTS), shock waves from nuclear test shots caused considerable damage in Las Vegas (66 miles away) and Indian Springs (24 miles away). Although damage was confined to shattered windows and cracked plaster, it was clear that continued damage could prohibit use of the continental test area. In consequence, Sandia Corporation Weapons Effects Department was assigned to provide forecasts of long-distance blast effects prior to each shot of subsequent test operations.*

At the time of Operation Upshot-Knothole, long-distance blast prediction had been developed only to a qualitative level—and predictions, based on scaling from pretest high-explosives (HE) shots, were not considered wholly adequate. Data recorded during Upshot-Knothole, from nuclear and HE explosions, were carefully studied to derive quantitative prediction methods. Satisfactory solutions to the many facets of the problem finally were obtained shortly before Operation Teapot began in the spring of 1955. Reporting the Upshot-Knothole program was therefore delayed to include refinements and verifications obtained in the 1955 program.

Weather conditions at NTS during Operation Upshot-Knothole were unseasonable; ie, the average temperature for May was an all-time recorded low.[4] (Departure of mean temperature for March-May 1953 is shown in Fig. 1.1.) In addition, a jet stream hovered over or near the test area throughout the series. Fortunately, orientation of this high-speed air stream on test dates did not support propagation of significantly damaging shocks into any nearby cities. On several occasions, conditions were borderline but, luckily, only twice did overpressures measured in Las Vegas, the nearest city, reach the minimum level for damage. Peak overpressure measurements at Las Vegas for all tests except Operation Ranger are plotted against shot yield in Fig. 1.2. Note that almost damaging shocks were observed on several occasions and from shot yields as small as 1 kt.

---

*Historical and theoretical details of the problem of observing and predicting air shocks at large distances from explosions have been published in earlier reports on Operations Buster-Jangle[1] and Tumbler-Snapper[2] and, with minor theoretical changes and corrections, in Reference 3. To avoid repetition, familiarity with these reports is frequently assumed in this report.

Fig. 1.1 -- Departure of Mean Surface Temperature from Normal, March-May 1953, Upshot-Knothole

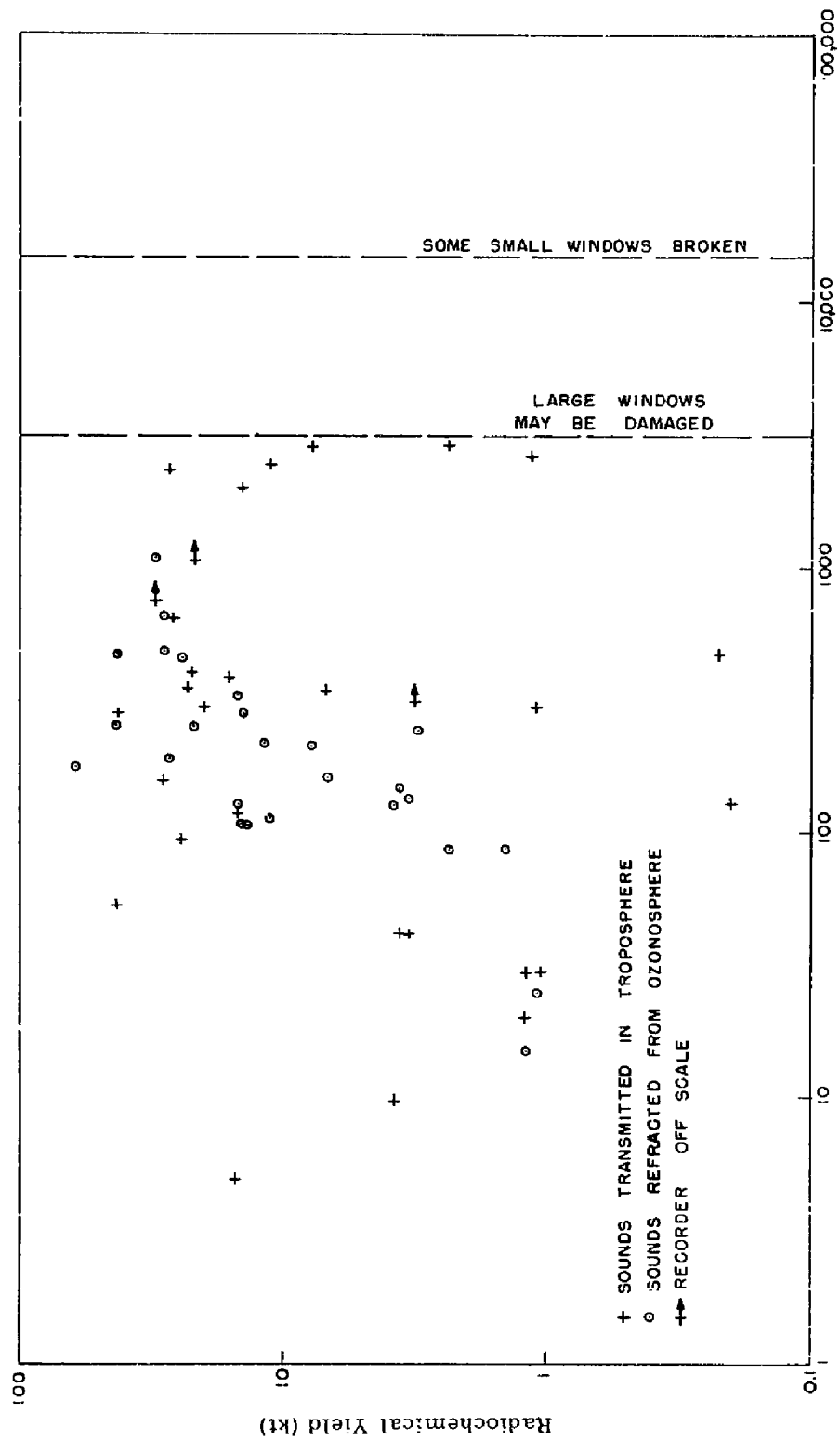

Fig. 1.2 -- Peak Pressures Measured at Las Vegas for All Tests Except Ranger

As in previous test series in Nevada, several checks were made prior to each shot to estimate magnitudes and destructive effects of pressure waves reaching inhabited regions outside the test site. On the basis of predictions of atmospheric temperature and wind structure provided by the Air Weather Service at staff briefings on evenings before shots, theorectical sound propagation patterns were developed. These patterns were adjusted during the night, as later measurements of atmospheric behavior were obtained. Two hours before a scheduled nuclear shot a 1.2-ton HE charge was detonated, and the sound was recorded at fifteen microbarograph stations circling the test area in Nevada, Utah, and California. At minus one hour another 1.2-ton HE shot was fired, and the records were checked for any late indication of serious consequences to be expected from detonation of the nuclear shot. Even when these multiple checks were made, predicted pressures were often considerably in error but, as previously indicated, no heavy damage occurred.

On Upshot-Knothole, however, 98 claims for blast damage were received by the Las Vegas Branch Office of the Atomic Energy Commission, some from points as remote as Modesto and Visalia, California, although the majority were from Las Vegas. This total is to be compared with 27 on Ranger, 294 on Buster-Jangle, and 132 on Tumbler-Snapper. All but one of the 98 were clearly insupportable and were denied.[5/] The one claim which received some consideration was from Las Vegas and was for a plate-glass window, possibly broken during a borderline peak-to-peak pressure condition of about 3.5 mb, but it was denied on the basis of faulty installation of the glass.

At Groom Mine, about forty miles northeast of the test area, a number of small windows were broken on Shots 8 and 10. On Shot 8, no actual pressure measurements were made at that point, but on Shot 10 a mobile microbarograph recorded a peak-to-peak surge of 15 mb. On both occasions, a strong shock had been predicted, and necessary precautions were taken to protect local inhabitants from injury. Damages were repaired by informal arrangement with the AEC test manager.

The strongest shock felt by observers at the Control Point during the entire series was on Shot 7. Although a microbarograph was not operated at the Control Point, an overpressure of 28.6 mb was measured by a Sandia experimental differential pressure transducer.[6/] Eleven millibars were recorded at the Transmitter Farm, where overpressures are usually less than half those at the Control Point. This shot caused noticeably higher overpressures than Shot 11, which struck the Control Point with about 22.8 mb.

On Shot 8, at Frenchman Flat, peak-to-peak pressure measured at Camp Mercury (Quonset 28) was 20.6 mb, and a number of small windows were broken there.

From data such as these examples, we infer that large plate-glass windows are damaged by peak-to-peak pressure pulses of about 3 mb; damage gradually increases with pressure level until at 15-20 mb small window panes are broken.

During Operation Teapot, weather conditions were again more than normally disturbed, but no month was so anomalous as May 1953. The departure of mean temperatures for February-May 1955 is shown in Fig. 1.3. High-speed jet stream winds were only occasionally observed in Southern Nevada. The operational program was changed by a greater emphasis on safety from radioactive fallout: thus, the apparent importance of a blast prediction program was reduced, although it certainly could not be overlooked. In general, high wind conditions, which could have caused serious blast propagation, were deemed too risky because they would have carried fallout in narrow intense bands to relatively great distances. However, on some occasions, when fallout patterns were forecast to lie toward the uninhabited "slot" to the southeast, tests were considered which might, if carried out, have created considerable blast disturbance in the Las Vegas area. Whenever winds were high enough to give strong tropospheric blast propagation, wind direction changes during the night prior to the planned shot caused cancellation.

The three air bursts of Teapot were small-yield weapons, so fallout was of relatively minor importance. Upper winds for these three shot dates did not support damaging shock propagation.

The blast prediction program was operated as in earlier test operations, and weather forecasts provided by Air Weather Service personnel were used to compute predictions of sound propagation patterns. However, Raypac* [7] was used for pattern prediction and made computation much simpler than before. In earlier tests, great masses of hand computations were required for even a rough quantitative estimate of the situation. Raypac, in about an hour of operating time, could produce a complete picture of the pattern in adequate detail for confident predictions. It became possible to make repeated checks based on actual upper air weather observations made at frequent intervals during the early morning hours before a test. Use of the analogue computer system is described in detail in Section 3.4.

Preliminary 1.2-ton HE shots were continued at 1 and 2 hours before full-scale tests. However, when complex propagation conditions existed, the Raypac-computed blast prediction was usually superior to predictions made by scaling HE results, because a complete pattern was available and probable weather variations for the last hour or two before shot time could be considered. Also, the possibilities for additive interference of signals of long duration,

*Ray Path Analogue Computer (developed at Sandia Corporation by Division 5413).

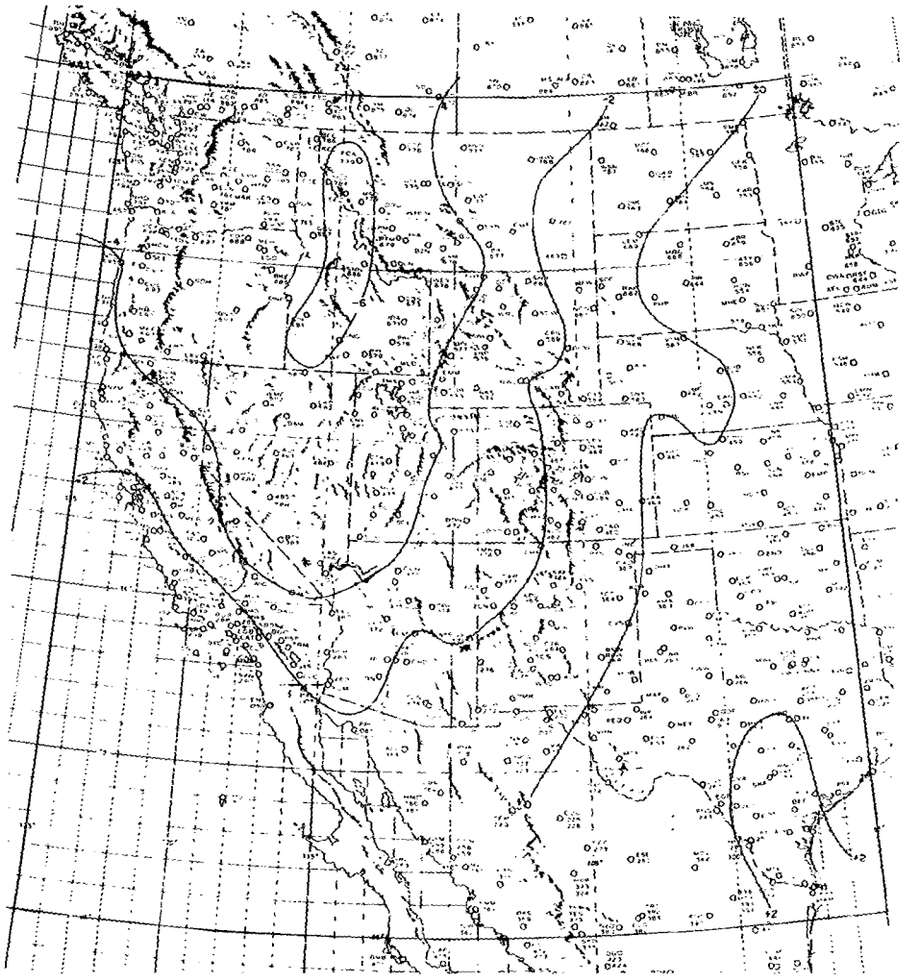

Fig. 1.3 -- Departure of Mean Surface Temperature from Normal, February-May 1955, Teapot

associated with large-scale blasts, could be included. Nevertheless, for ozonosphere signals, HE scaling techniques remained the only predictors.

In summary, blast protection for the surrounding regions was well provided. At Las Vegas, the maximum overpressure observed from a Teapot test was from Moth shot and was 1.55 mb (about 20 per cent below the minimum level for damage). Informal reports of minor damage to plaster were received, but there were no significant damage claims from the Las Vegas area.

Ozonosphere signals above damaging minimums were observed at St. George, Utah. Turk shot caused 3.4 mb overpressure, Bee gave 1.9 mb, and Met gave 4.0 mb. There was a report of a previously cracked window being knocked out, but no claims were made. Evidently the slower pressure rise rate of these particular ozonosphere signals may have allowed larger peak pressures without the damaging effects found with waves ducted through the troposphere.

The only significant blast-damage claims from the operation were from turkey farmers in the region of Fresno and Bakersfield, California. One, living near Bakersfield, claimed that noise from Apple II shot stampeded his 5000 turkeys into the pen fences, suffocating and killing 600 and causing the feeding schedule of the others to be disrupted. After Zucchini shot, a similar occurrence was not so disastrous because the farmer had had prior news of the planned test and had alerted help to break up the stampede when the blast noise arrived. A settlement of this claim may have led a Fresno claimant to file similar charges, but on the dates he claimed damages were sustained, Inyokern and Bishop microbarographs recorded only 10-20 per cent of the noise levels measured from Apple II and Zucchini shots.

An abnormally strong shock, ducted beneath a strong surface-temperature inversion from Turk shot toward the open shot area, demonstrated the effects of 0.5 psi, or 35 mb, overpressure on housing. In the FCDA houses most windows were shattered, doors were torn off, and other damages were sustained. Surprisingly, only a few panes side-on to the blast and lee side from the blast were broken, but nearly all front windows were broken out, with fragments blown through rooms and embedded in the far walls. Obviously, considerable injuries to personnel would have been sustained under these conditions if no precautions had been taken. This pressure level could be expected 45 miles from a 20-mt burst.

Experiments conducted with dwelling-size panes of glass mounted under the HA (High-Altitude) shot showed that, at least at 9 mb overpressure, windows up to 2 feet square were not broken. However, under actual conditions found in a city, many such panes are held in place by old dried putty or less secure frame fasteners and would be shattered by this blast

pressure. Further, in one case of atmospheric focusing, 9 mb overpressure was predicted for Las Vegas at a preliminary briefing session. This particular test approach was finally canceled because of fallout hazard but, from the point of view of blast damage, this was an example of the kind of prediction the Weapons Effects Department was prepared to make.

In addition to their primary use in blast prediction, microbarograph observations of blast pressure signals provide data on sounds refracted to the ground from the ozonosphere. This information is used to operate the blast prediction system in reverse, providing observations of atmospheric conditions in the 100,000- to 150,000-foot levels. During Operation Castle, where long-distance blast prediction is of little interest, microbarographs were operated primarily to obtain data on ozonosphere conditions. Derivations and results of sound probing of the ozonosphere for all three operations are detailed in Chapter 5.

CHAPTER 2

INSTRUMENTATION

Microbarographs used by Sandia Corporation in Operations Buster-Jangle and Tumbler-Snapper were borrowed from the U. S. Naval Electronics Laboratory. In Upshot-Knothole and later operations, new Wiancko-type 3-PBM-2 microbarographs[6] were used. (Typical instrumentation setups for Castle and Teapot are shown in Figs. 2.1-2.4.) Their sensitivities were stepped for several values of peak amplitude ranging from ±4 μb to ±12 mb. Each range also had a quarter-scale output. Recordings were made on Brush two-channel recorders. Pressure records were thus available for scales ranging from 0.2 μb/mm to 2400 μb/mm. Measurement was theoretically possible for signal amplitudes of from 0.2 μb to 96 mb but, since ambient wind noise gives pressure waves of 10- to 100-μb amplitude, only under absolutely calm conditions could signals of below 10 μb be detected. At 0445 PST, February 22, 1955, however, a discernible signal from an HE shot was recorded at Boulder City, with only 0.48-μb peak-to-peak amplitude.

At the other extreme, UK-7 shot gave recordings of 22.8 mb at the control point, and Apple II shot of Teapot gave peak-to-peak pressure of 21.3 mb. Teapot Turk shot records show pressure amplitude of only 15 mb, but the building which housed the recording system was so shaken that the record was cut off. When checked against other Sandia Corporation pressure measurements on Teapot HA shot, microbarograph amplitudes were in agreement within 20 per cent.[9]

Eighteen microbarograph units were installed and operated during Upshot-Knothole (in addition to a development model set up at Albuquerque and production spares operated by Wiancko Engineering, Inc., at Pasadena, California). Some changes in operating location were made during the test series, and a mobile unit—Skippy—was available for on-call operation at points determined from preliminary forecasts. In an attempt to establish characteristics of signals refracted to earth from the ozonosphere (30-60 km) and ionosphere (above 90 km), dual installations were made at six points. Maps of NTS and the surrounding area are presented (Figs. 2.5 and 2.6) to indicate operating locations of the various microbarograph installations and shot points for HE and nuclear test shots.

For Operation Teapot, the eighteen units were rearranged to improve the collection of ozonosphere signal data. Figure 2.7 shows map locations of regularly operated recorders.

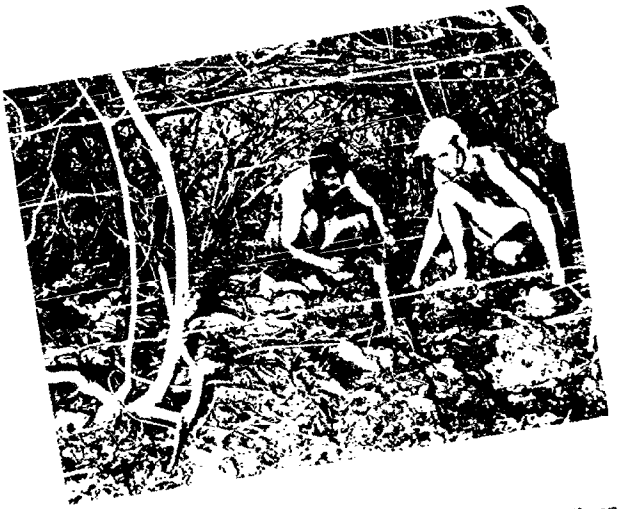

Fig. 2.1 -- Microbarograph Sensing Head on Glenn, Eniwetok Atoll, Castle

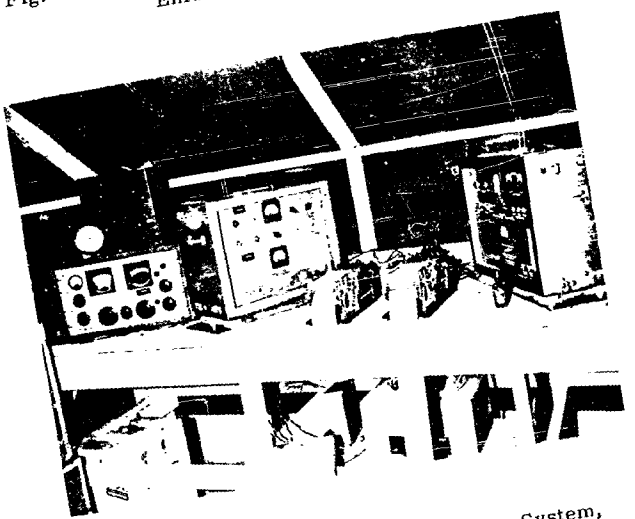

Fig. 2.2 -- Microbarograph Recording System, Eniwetok, Castle

Fig. 2.3 -- Microbarograph Sensing Head at Boulder City, Teapot

Fig. 2.4 -- Microbarograph Recording Station, Boulder City, Teapot

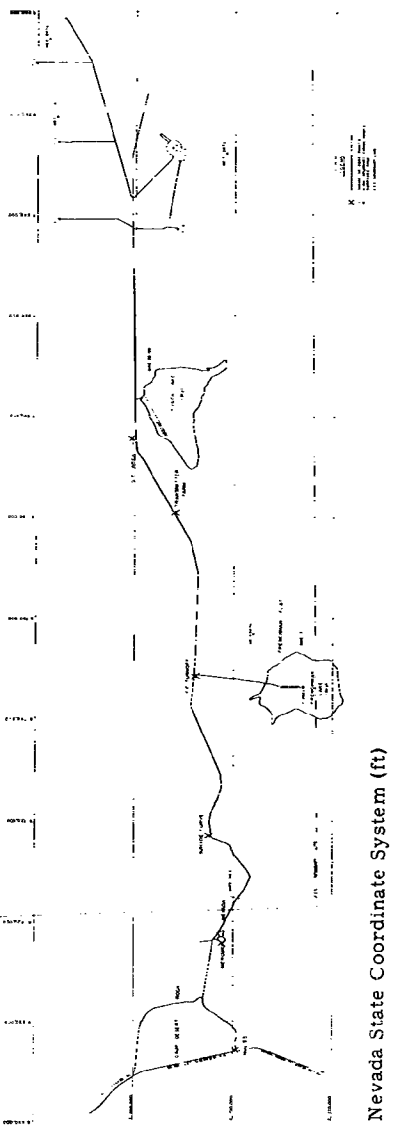

Fig. 2.5 -- Microbarograph Stations and Nuclear and HE Shot Points at the Nevada Test Site, Upshot-Knothole

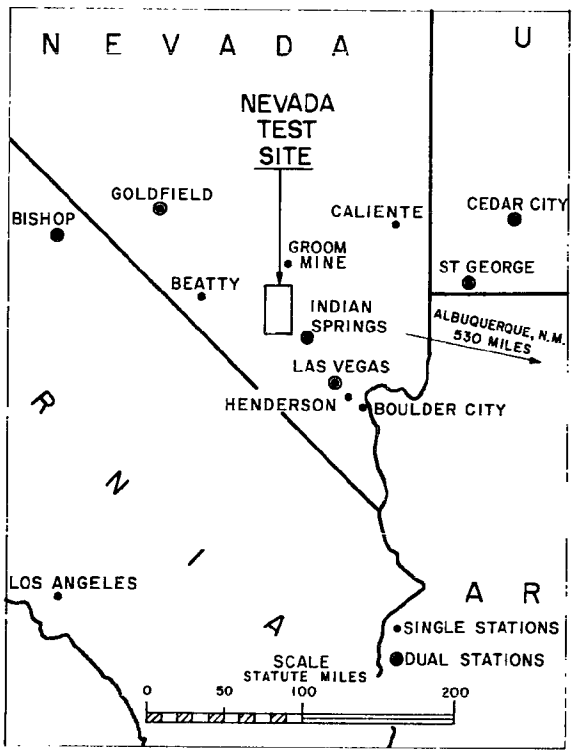

Fig. 2.6 -- Microbarograph Recording Stations Used During 1953, Upshot-Knothole

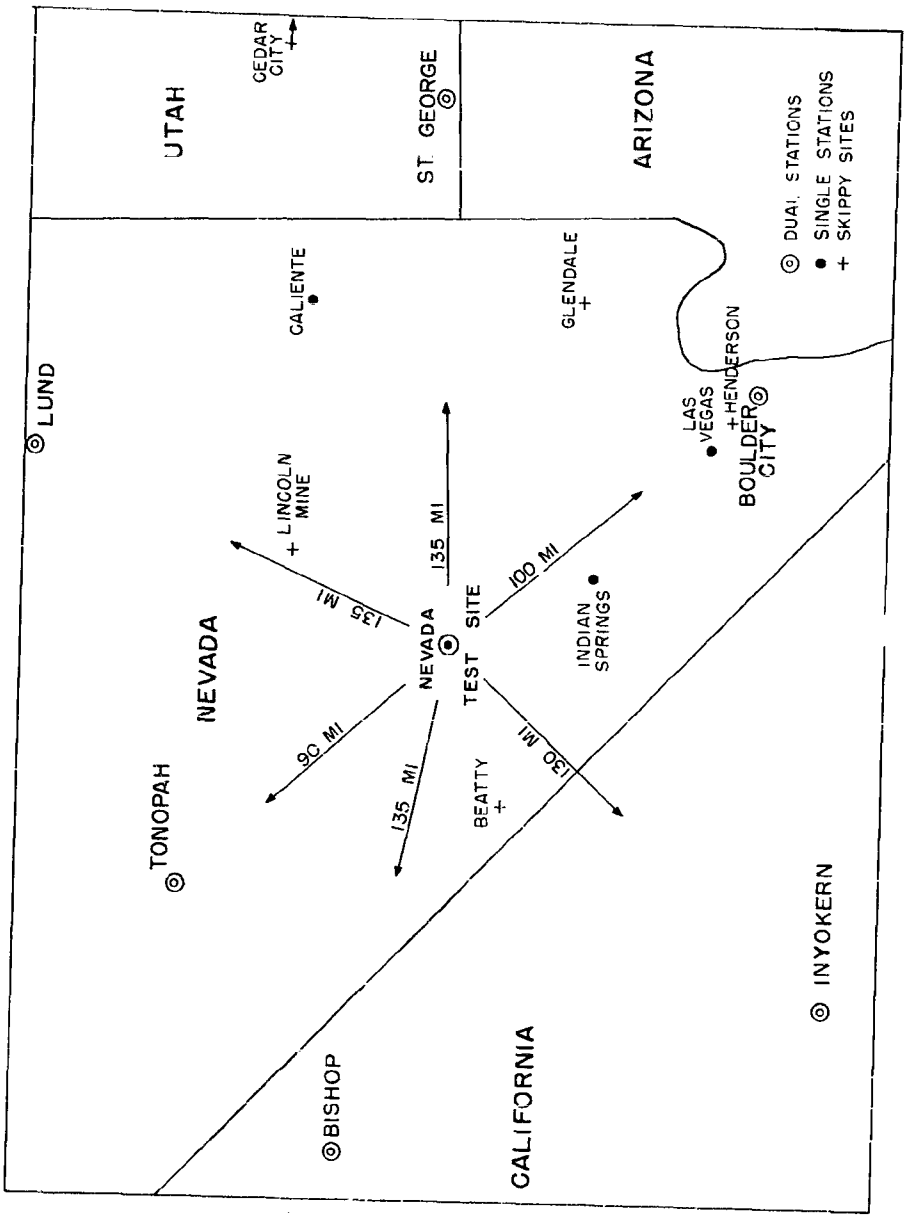

Fig. 2.7 -- Microbarograph Recording Stations Used During 1955, Teapot

As before, one unit was equipped for mobile operations and, at various times, recorded at locations indicated on the map.

Only one equipment modification was tried during Teapot. An experimental 50-kc broad-band radio receiver was connected to the recorder to give an automatic zero-time indication from the electromagnetic transient of the bomb burst.[10] This scheme worked with only fair reliability, but proved in principle that an automatic zero-time indication was possible for most types of atomic bomb tests. In future programs, a refined automatic zero-time indication will be used to aid in communicating the occurrence or cancellation of a test to distant operators, since WWV-based time indications are not always received.

Microbarographs were operated on Operation Castle to record pressures at observer areas and measure ozonosphere signals.[11] Station locations are shown in Fig. 2.8.

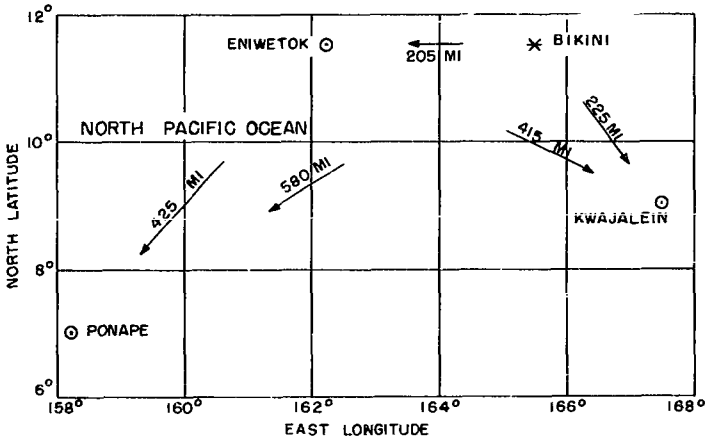

Fig. 2.8 -- Microbarograph Recording Stations Used During 1954 Operation Castle

CHAPTER 3

PREDICTING SIGNAL PROPAGATION

3.1 GENERAL CONSIDERATIONS

Atmospheric signal ducts are essentially of three types. First, and in some respects simplest for sound-propagation analysis, are signals ducted under a surface temperature inversion, as in Fig. 3.1. Next, the so-called complex case, where sound velocity decreases with height above ground level, then increases to a value above that at ground, as shown in Fig. 3.2. On occasion, further zigzags of the velocity–height structure occur. Finally, there are signals refracted from the ozonosphere and ionosphere, essentially complex cases, which preclude analytical prediction because they travel unknown regions of the atmosphere. However, these may be scaled, with reasonable success, for pressures from smaller pretest high-explosives shots.

Peak overpressure, P, for continuous sinusoidal acoustic waves may be expressed by[1]

$$P = (2\xi\rho V/\tau)^{1/2}, \tag{3.1}$$

where ρ is the air density, V is the velocity of propagation, ξ is the surface density of direct energy, and τ is the duration of the constant amplitude signal. In turn, ξ is defined by

$$\xi = \frac{W\epsilon}{2\pi R} \cot \theta_o \frac{d\theta_o}{dR}, \tag{3.2}$$

where W is the total blast energy, R is the distance from the explosion, and θ_o is the initial latitude angle on the sphere of the explosion of a ray returned to earth at distance, R; ϵ is the fraction of released energy which remains as acoustical energy after the blast wave has traversed the horizontal distance to R. Near an explosion, nonadiabatic processes[12, 13] of shock wave propagation leave behind, in the form of heat, much of the originally released energy. An experimentally determined value[14] of ϵ, satisfactory for ratios of $R/W^{1/3} > 0.128$ ft/(kt Nu)$^{1/3}$, Nu meaning nuclear, is

$$\begin{aligned} \epsilon &= 4.7 \times 10^{-2} + 5.7 \times 10^{-4} \text{ (W, kg HE)}^{1/3}/\text{(R km)} \\ &= 4.7 \times 10^{-2} + 2.7 \times 10^{-2} \text{ (W, kt Nu)}^{1/3}/\text{(R miles)} . \end{aligned} \tag{3.3}$$

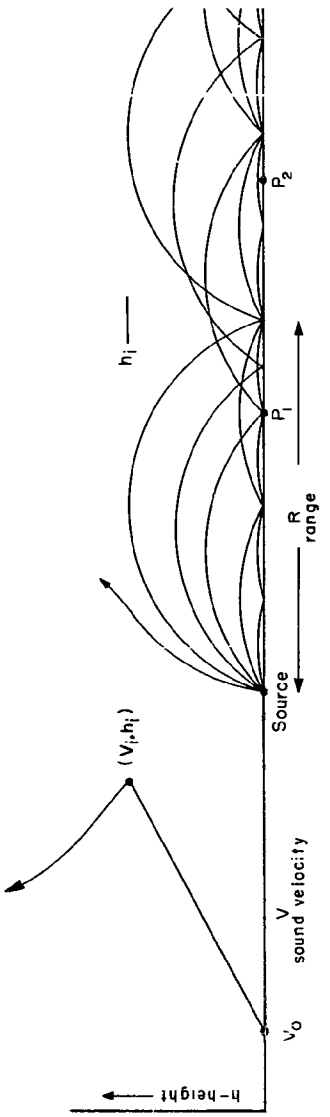

Fig. 3.1 -- Sound Ray Paths Under a Surface Temperature Inversion

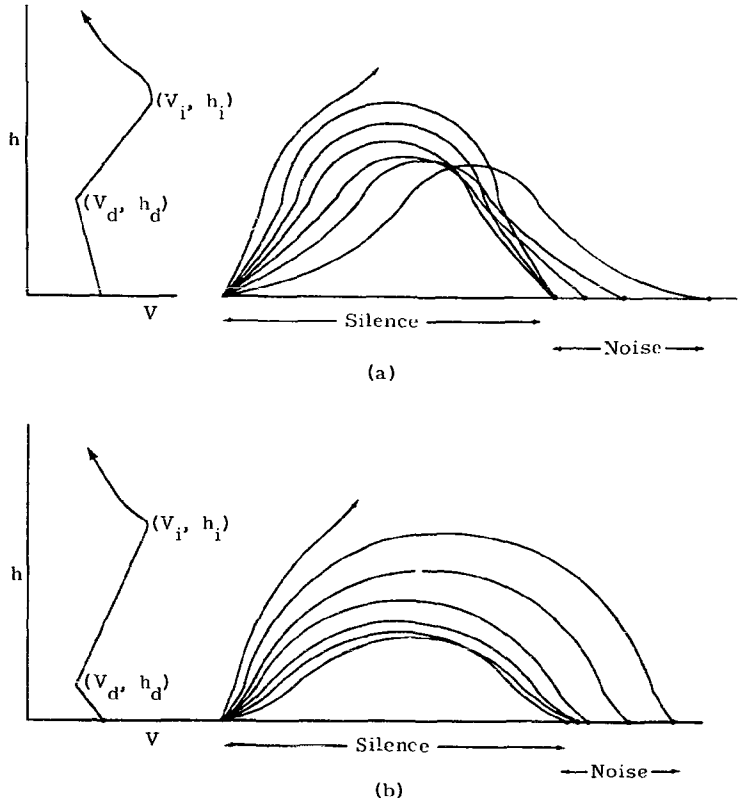

Fig. 3.2 -- Sound Ray Paths for the Complex Atmospheric Case, with a Focus of Energy

Thus, except for places close by large explosions, this "efficiency" factor is 4.7 per cent.

At successive skip distances outward along its path, the energy of an acoustic wave will be further reduced by absorption and dispersion. Equations 3.1 and 3.2 show that after n cycles through the atmosphere, overpressure due to a single incremental initial solid angle, since at R the pressure is reinforced by reflection, may be expressed by

$$P^2 = \frac{\rho_o V_o W \epsilon f^{n-1}(1+f)}{\pi \tau R} \cot \theta_o \frac{d\theta_o}{dR} . \qquad (3.4)$$

The fraction of incoming acoustic energy reflected from the ground surface into the atmosphere at each strike is indicated by f.

3.2 PROPAGATION UNDER AN INVERSION

When sound velocity increases linearly with altitude to the top of the inversion at height, h_i, and decreases thereafter, the limiting ray, starting at θ_o = arc cos V_o/V_i and becoming horizontal at h_i, strikes the earth at a distance[1]

$$R_{max} = 2h_i \sqrt{\frac{V_i + V_o}{V_i - V_o}} \approx 2.8 h_i \sqrt{\frac{V_o}{V_i - V_o}} . \qquad (3.5)$$

Furthermore, under the inversion, at $R \leq R_{max}$,

$$\frac{dR}{d\theta_o} = \frac{R}{\sin \theta_o} . \qquad (3.6)$$

Total incident sound intensity at a point on the ground consists of that coming directly from the source, plus that received after one reflection from an area one-fourth as large at half the distance, plus that received after two reflections from an area one-ninth as large at one-third the distance, etc. If it is assumed that all impulses arrive at R at about the same time, then overpressure may be expressed by

$$P^2 = \frac{\rho_o V_o W \epsilon}{\pi \tau R^2} \cos \theta_o (1+f) \sum_{n=N}^{n=\infty} f^n = \frac{\rho_o V_o W \epsilon}{\pi \tau R^2} \cos \theta_o \left(\frac{1+f}{1-f}\right) f^N , \qquad (3.7)$$

where N is the whole number of times R_{max} divides into R, or the number of completed cycles over the atmospheric path touching the top of the inversion.

Little experimental and no known theoretical effort has been directed toward determining effective signal duration. Reasonable values of τ, as observed at overpressures less than

five per cent of a standard atmosphere, appear to lie, for the linear inversion situation, between two limiting equations,[15]

$$\tau_1 = 3.3 \times 10^{-2} \text{ (W, kg HE)}^{1/3} \text{ sec} = 2.54 \text{ (W, kt Nu)}^{1/3} \text{ sec}, \quad (3.8)$$

and

$$\tau_2 = 9.3 \times 10^{2} \text{ (W, kg HE)}^{1/6} (R_{max}, \text{ km})^{4.2} \text{ (R, km)}^{1/2} \text{ sec} = 1.4 \times 10^{3} \text{ (W, kt Nu)}^{1/6} (R_{max}, \text{ mi.})^{-4.2} \text{ (R, mi.)}^{1/2} \text{ sec}. \quad (3.9)$$

For more complex situations, a slightly different coefficient for Eq 3.8 is used and will be discussed later.

Similarly, little effort has been devoted to determining the energy reflection factor, f, over real terrain. Reflection from a smooth air-to-topsoil surface density discontinuity should be 99.7 per cent.[15] Destructive interference apparently reduces f significantly below this ideal value, and in experiments under surface inversions at NTS, the value of f appears to lie between 60 and 75 per cent.

By joining these not-very-well-determined empirical values, and considering nuclear blast yield to be one-half the blast yield of an equivalent tonnage of high explosives, two expressions are obtained for predicting peak overpressure for the linear inversion situation:

$$P_1 = 40.3 \text{(W, kt Nu)}^{1/3} (0.75)^{N/2}/\text{(R, mi.) mb} \quad (3.10)$$

and

$$P_2 = 1.2 \text{(W, kt Nu)}^{0.415} (R_{max}, \text{ mi.})^{2.1} (0.6)^{N/2}/\text{(R, mi.)}^{1.25} \text{ mb}. \quad (3.11)$$

Graphs of these two equations for a typical HE explosion are shown in Fig. 3.3.* Observed peak pressures lie between these limiting graphs.

3.3 PROPAGATION IN COMPLEX ATMOSPHERES

A satisfactory system was also derived for predicting sound propagation under more complex atmospheric conditions, with minor changes in constants and assumptions from those used in developing the inversion case. Previously, it had been assumed that differences in arrival times of sound signals arriving by various paths were insignificant compared to other

*Reproduced from Reference 15.

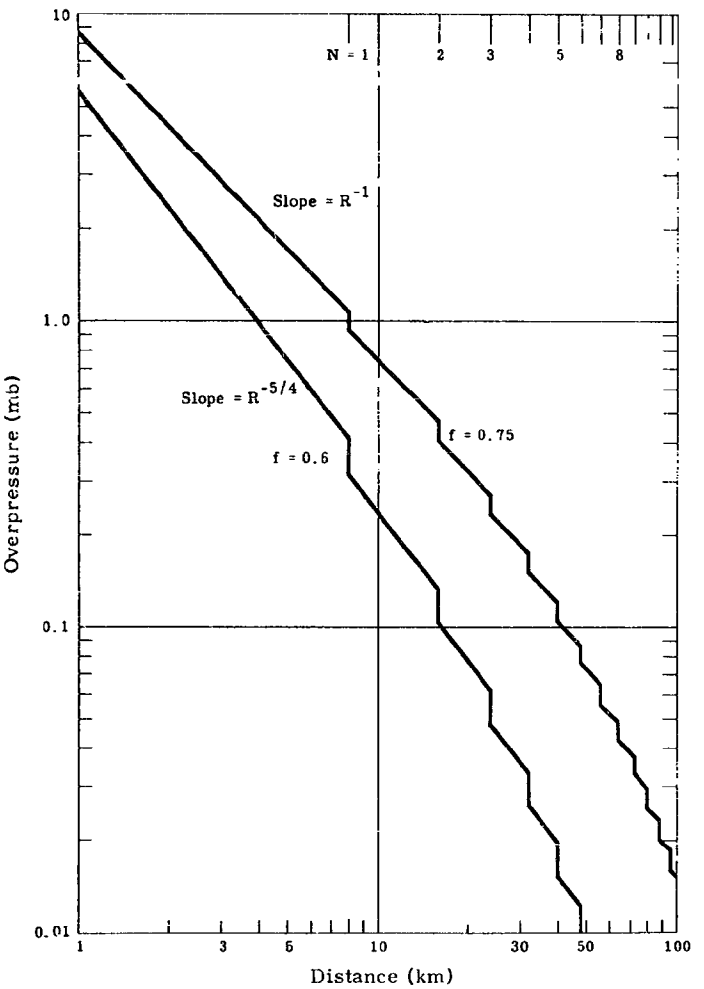

Fig. 3.3 -- Peak Overpressure versus Distance from a Surface Explosion Under an Inversion

errors in determining paths and characteristics of atmospheric sound patterns. Considerable difficulty had always been encountered in predicting exact (±1 second) arrival times of shock signals at large distances. Consequently, it had been assumed[1] that impulses arriving at a point by various paths will undergo direct additive interference, and it had been deduced from the appearance of recordings that single impulses of explosive shocks break down into acoustic pressure wave trains.

More detailed investigation of the situation has revealed that relative arrival times of impulses following different paths through the atmosphere may be determined successfully. Separation time between arriving signals was often found to be appreciable when compared with the fundamental period of the initiation explosion. In fact, arrival times of signals reaching Las Vegas by different routes through the lower (25,000 feet) troposphere may differ by 10 to 15 seconds. Under a surface inversion, arrivals by different paths will be spread over not more than 5 seconds. Only when distance traveled is less than twenty miles for nuclear tests may time separation be completely ignored and the cumulative effect procedure be applied without question. On the other hand, treatment of overpressures as separate impulses requires more detailed consideration of the estimated reflection and period terms in a peak overpressure equation similar to Eq 3.4.

A Fourier analysis of some Upshot-Knothole microbarograph records was performed by REAC to determine maximum energy frequency components of individual records. Spectral curves of relative occurrence versus frequency were averaged for several stations on each of several shots of different yields in the Upshot-Knothole series. Results are shown in Fig. 3.4, with an RMS fitted line for all shots analyzed, following the relation that period,

$$\tau = 2.836\ (W,\ \text{kt Nu})^{1/3} . \qquad (3.12)$$

Reasonable agreement with Cowan's[16] results is shown.

Energy flux, Eq 3.2, is proportional to $d\theta_o/dR$, which requires systematic evaluation as a function of the various atmospheric layers the signal has passed through. At first return to the ground, n = 0; this rate may be found in inverse form, $dR/d\theta_o$, by differentiating the ray-path equation,[1]

$$R_{i+1} - R_i = \frac{h_{i+1} - h_i}{V_{i+1} - V_i} \left[\sqrt{V_p^2 - V_i^2} - \sqrt{V_p^2 - V_{i+1}^2} \right] . \qquad (3.13)$$

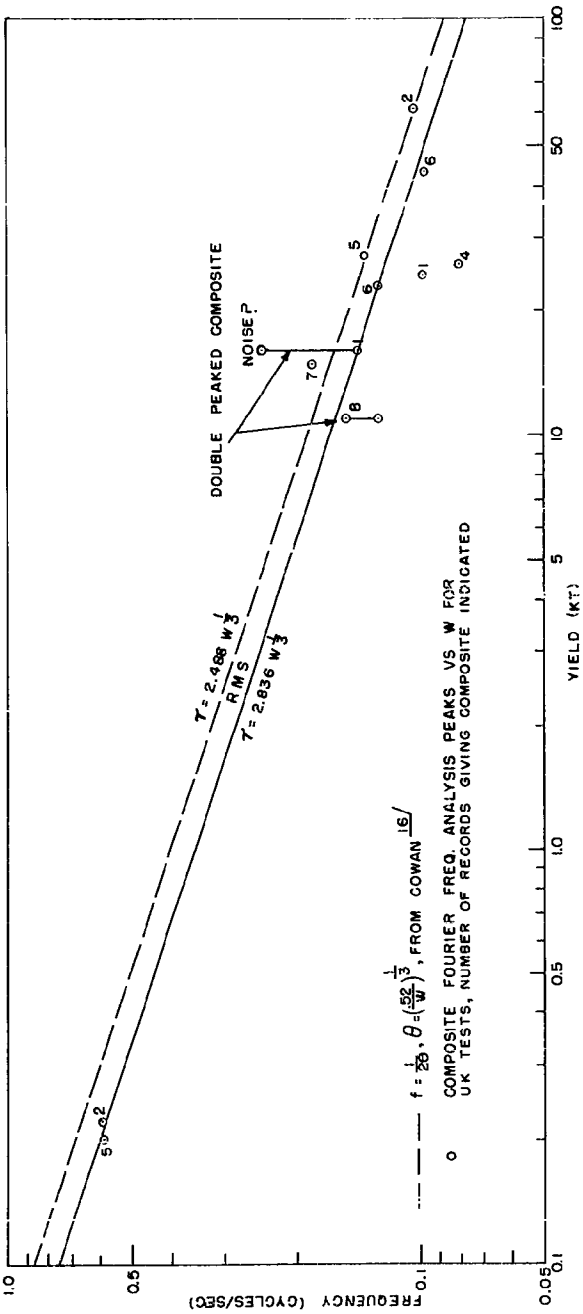

Fig. 3.4 -- Sound Signal Frequency versus Yield for Upshot-Knothole Tests

When multiplied by some of the other atmospheric variables in Eq 3.4, the contribution to divergence of energy due to passing twice through each layer, $h_{i+1} - h_i$, once upward and then downward, when $V_i \neq V_{i+1}$, is

$$\frac{1}{V_o} \tan \theta_o \frac{d(R_{i+1} - R_i)}{d\theta_o} = - \frac{V_p^2 \left(V_p^2 - V_o^2\right)}{V_o^3} \cdot \frac{(R_{i+1} - R_i)}{\sqrt{\left(V_p^2 - V_i^2\right)\left(V_p^2 - V_{i+1}^2\right)}} . \qquad (3.14)$$

An indeterminate form is not reached when $V_{i+1} = V_p$, since $\sqrt{V_p^2 - V_{i+1}^2}$ is zero, and its derivative, as shown here, is also zero, not infinity. Instead, when $V_{i+1} = V_p$,

$$\frac{1}{V_o} \tan \theta_o \frac{d(R_p - R_{p-1})}{d\theta_o} = - (R_p - R_{p-1}) \frac{V_p V_{p-1}}{V_o^3} \cdot \frac{V_p^2 - V_o^2}{V_p^2 - V_{p-1}^2} . \qquad (3.15)$$

The case where $V_i = V_{i+1}$ is not special, as it is in ray tracing, but here

$$\frac{1}{V_o} \tan \theta_o \frac{d(R_{i+1} - R_i)}{d\theta_o} = - (R_{i+1} - R_i) \frac{V_p^2 \left(V_p^2 - V_o^2\right)}{V_o^3 \left(V_p^2 - V_i^2\right)} . \qquad (3.16)$$

Thus, for a complete path through the atmosphere and back to ground

$$\frac{1}{V_o} \tan \theta_o \frac{dR}{d\theta_o} = 2 \frac{V_p^2 \left(V_p^2 - V_o^2\right)}{V_o^3} \left[\sum_{i=0}^{i=p-2} \frac{R_{i+1} - R_i}{\sqrt{\left(V_p^2 - V_i^2\right)\left(V_p^2 - V_{i+1}^2\right)}} + \frac{V_{p-1} (R_p - R_{p-1})}{V_p \left(V_p^2 - V_{p-1}^2\right)} \right] . \qquad (3.17)$$

This equation may be evaluated from many of the same terms used in computing ray-path distances. In this manner, microbarograph observations of overpressures at ranges from the NTS control point to Boulder City were analyzed for two cases of complex atmospheric conditions encountered during Operation Upshot-Knothole. Eighteen station measurements were found to yield RMS values for $f = 0.936$ and for $\epsilon = 0.0281$. This value for reflection coefficient is considerably nearer to a theoretical topsoil reflection factor than was derived for inversion conditions in Section 3.1, but data scatter and the predominant effect of varying the ϵ term do not allow strong confidence in the result. The ϵ factor, however, falls reasonably close to an extrapolation from the 100- to 1-psi pressure levels for nuclear blast curves.[17] Various sources[13, 17, 18] show considerable disagreement concerning the form of the adiabatic transmission coefficient (Fig. 3.5). However, sound waves, being adiabatic processes, should eventually acquire a constant energy level.

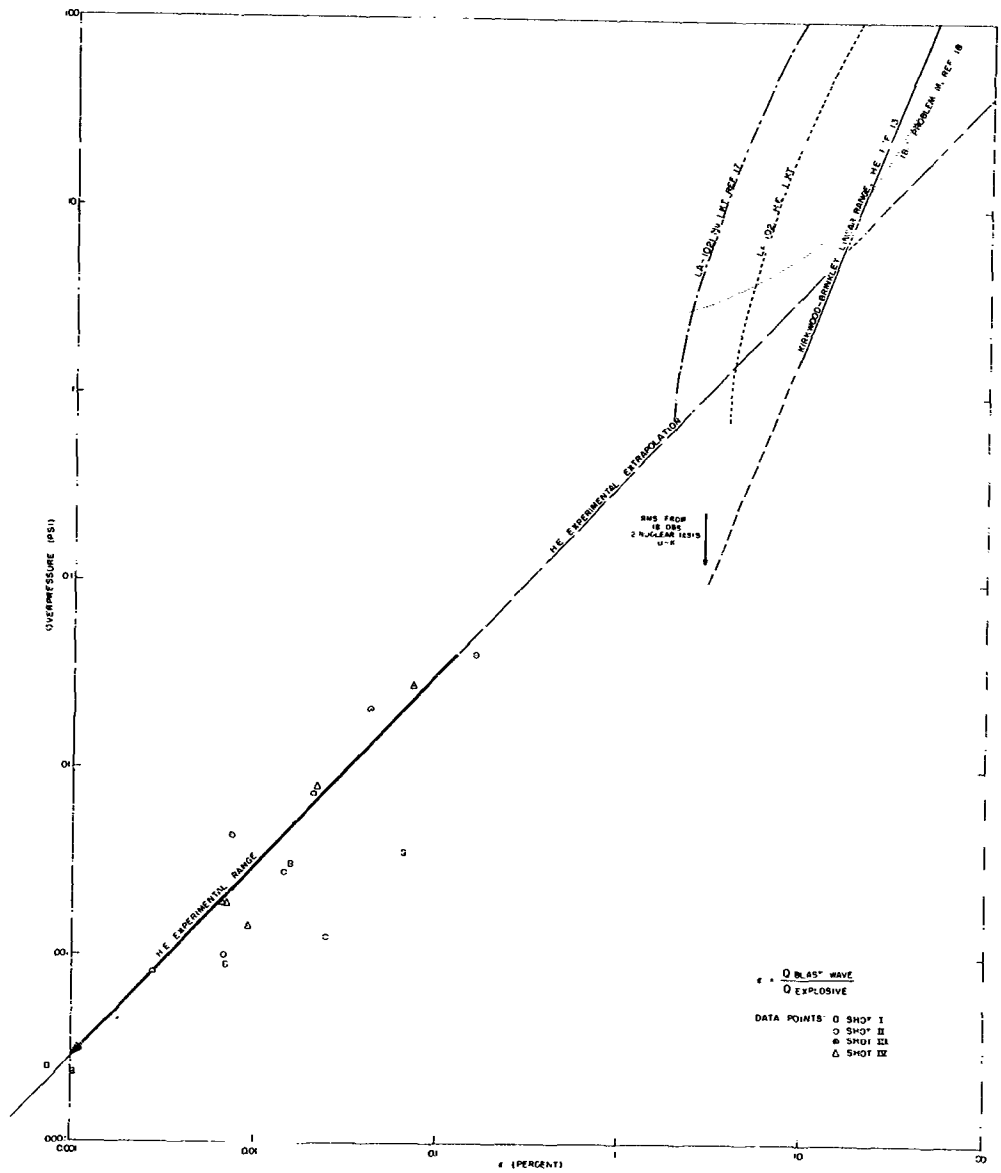

Fig. 3.5 -- Fraction of Initial Blast Energy Remaining in Shock or Sound Wave

3.4 RAYPAC PROPAGATION COMPUTATIONS

The Raypac computer, shown in Fig. 3.6, was being developed simultaneously with studies of Upshot-Knothole data, so the tremendous advantage of rapid pattern calculation was not available for determining the nonatmospheric quantities, ϵ and f. Construction of the machine was completed only shortly before the start of Operation Teapot and was not available for further research computations.

The computer is designed to take, as input data, the sound velocity versus altitude structure in a direction from a sound source. Hand calculations are not entirely eliminated at present. Rawinsonde weather observations and weather forecasts provide (at specified levels in the atmosphere) temperature, wind direction, and wind speed, plus other atmospheric parameters of no interest in sound propagation. For sound-ray plotting, therefore, temperature must be converted to sound speed, and the wind component in the direction of interest must be extracted from the total wind vector. Tables 3.1 and 3.2 are for calculating these necessary terms. Actually, the input is not sound velocity but, rather, the ratio of sound velocity at an altitude to sound velocity at burst height. This allows generalization to any burst height and simplifies the analogue function generator. Table 3.3 is an example of computations necessary to prepare actual inputs for the machine. After atmospheric data have been fed to the machine, paths of prescribed sets of rays may be plotted automatically. For filling in, additional rays may be drawn by manual entry of initial angle cosines. A new vertical-structure input and ray-path plot are necessary for each direction of interest, generally toward populated localities around the test site. Usually from 3 to 5 separate plots similar to Fig. 3.7 are adequate for a briefing forecast, and they are made only for directions in which upper-air sound velocity exceeds the surface value.

At first glance, a plot shows where sound will strike the ground and whether a blast will be heard. However, since each ray path is for a known initial elevation angle, the arrival spacing of successively inclined rays provides a $dR/d\theta_o$ measurement, $\Delta R/\Delta\theta_o$, for calculating overpressure. Experience has shown that even at distances nearly 100 miles from a large explosion, blast wave overpressure-time curves maintain an N-wave shape, similar to the close-in wave, rather than degenerate to sinusoidal form. In this case, the coefficient of Eq 3.1 is changed so that

$$P_{N\text{-wave}} = (3\xi\rho V/\tau)^{1/2} . \qquad (3.18)$$

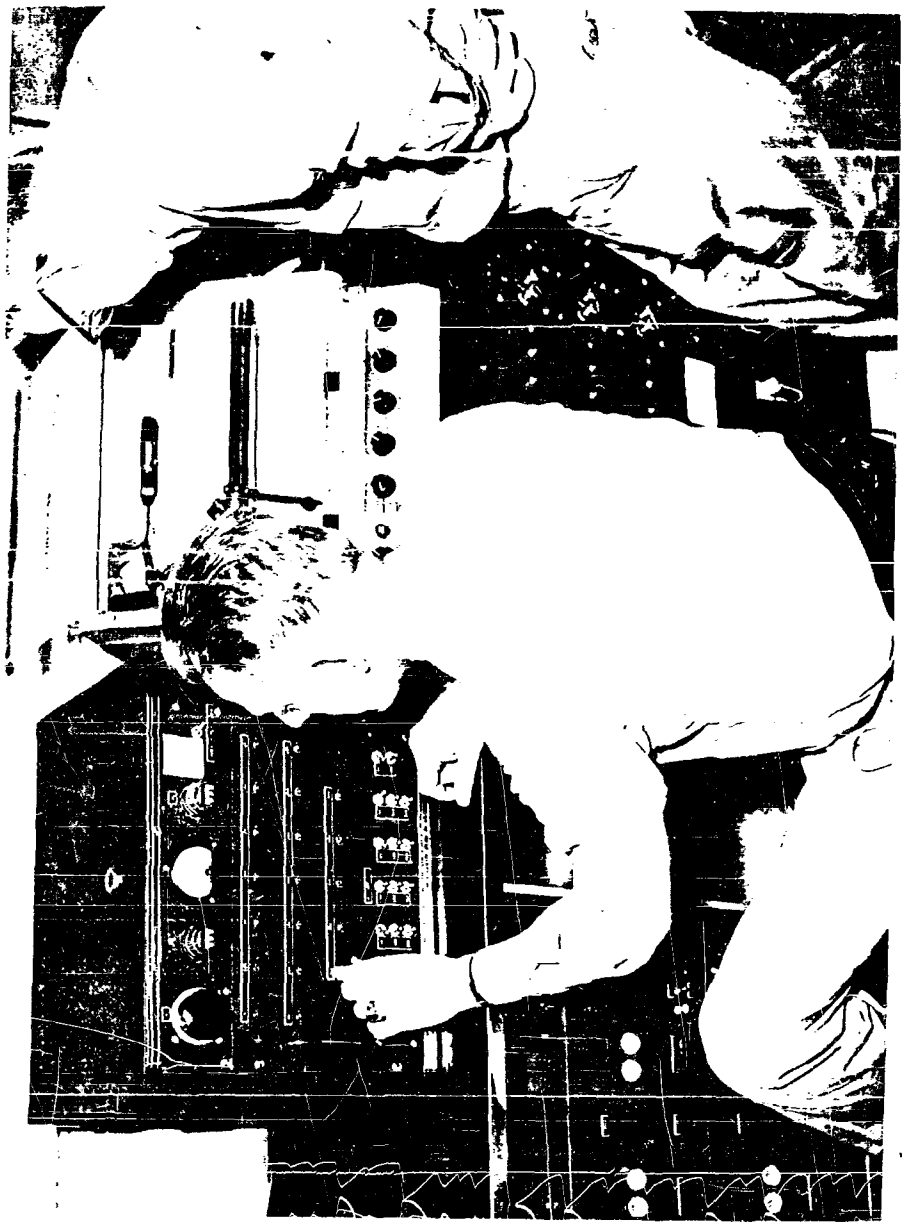

Fig. 3.6 -- Raypac Computer for Plotting Sound Rays

TABLE 3.1

Speed of Sound in Air
(ft/sec)

Temperature (°C) Tens \ Units	0	1	2	3	4	5	6	7	8	9
-80	914.8	912.4	910.0	907.6	905.2	902.8	900.4			
-70	938.3	935.9	933.6	931.3	929.0	926.6	924.3	921.9	919.6	917.2
-60	961.0	958.8	956.5	954.3	952.0	949.7	947.5	945.2	942.9	940.6
-50	983.2	981.0	978.8	976.6	974.3	972.1	969.9	967.7	965.5	963.3
-40	1005.0	1002.8	1000.7	998.5	996.3	994.1	992.0	989.8	987.6	985.4
-30	1026.4	1024.2	1022.1	1020.0	1017.9	1015.7	1013.6	1011.4	1009.3	1007.1
-20	1047.3	1045.3	1043.2	1041.1	1039.0	1036.9	1034.8	1032.7	1030.6	1028.5
-10	1067.9	1065.8	1063.8	1061.8	1059.7	1057.7	1055.6	1053.6	1051.5	1049.4
-0	1088.0	1086.0	1084.0	1082.0	1080.0	1078.0	1076.0	1074.0	1072.0	1070.0
0	1088.0	1090.0	1092.0	1094.0	1095.9	1097.9	1099.9	1101.9	1103.9	1105.8
10	1107.8	1109.7	1111.7	1113.6	1115.6	1117.5	1119.5	1121.4	1123.3	1125.2
20	1127.2	1129.1	1131.0	1132.8	1134.8	1136.7	1138.6	1140.5	1142.4	1144.3
30	1146.2	1148.1	1150.0	1151.9	1153.8	1155.6	1157.5	1159.4	1161.3	1163.1
40	1165.0	1166.9	1168.7	1170.6	1172.4	1174.2	1176.0	1177.8	1179.6	1181.4

SECRET

TABLE 3.2

Wind Resolution Coefficients

w = Observed wind speed, knots
W_H = Wind component, H = direction, ft/sec
D = True direction from which wind is blowing

$W_H = -1.689w \cos (D-H) = Gw$
1 knot = 1.689 ft/sec
1 knot = 1.15 mps

G

D° \ H°	Control Point Mercury	Indian Springs	Boulder City and Las Vegas	St George	Caliente	Lund	Tonopah	Bishop	Inyokern
	180°	149°	137°	86°	62°	23°	321°	281°	226°
360	+1.689	+1.447	+1.235	-0.118	-0.793	-1.554	-1.314	-0.322	+1.173
350	+1.664	+1.577	+1.416	-0.177	-0.522	-1.416	-1.478	-0.605	+0.945
340	+1.587	+1.658	+1.554	-0.466	-0.235	-1.235	-1.598	-0.870	+0.687
330	+1.462	+1.688	+1.647	-0.741	+0.059	-1.016	-1.669	-1.108	+0.409
320	+1.294	+1.669	+1.687	-0.994	+0.351	-0.767	-1.688	-1.314	+0.118
310	+1.086	+1.598	+1.677	+1.215	+0.633	-0.494	-1.658	-1.478	-0.177
300	+0.844	+1.478	+1.615	+1.400	+0.895	-0.206	-1.577	-1.598	-0.466
290	+0.578	+1.314	+1.505	+1.543	+1.130	+0.088	-1.447	-1.669	-0.741
280	+0.293	+1.108	+1.348	+1.639	+1.331	+0.380	-1.274	-1.688	-0.994
270	0	+0.870	+1.151	+1.684	+1.492	+0.661	-1.063	-1.658	-1.215
260	-0.293	+0.605	+0.920	+1.681	+1.606	+0.920	-0.819	-1.577	-1.400
250	-0.578	+0.322	+0.661	+1.624	+1.673	+1.151	-0.550	-1.447	-1.543
240	-0.844	+0.029	+0.380	+1.519	+1.687	+1.348	-0.264	-1.274	-1.639
230	-1.086	-0.264	+0.088	+1.367	+1.653	+1.505	+0.029	-1.063	-1.684
220	-1.294	-0.550	-0.206	+1.173	+1.566	+1.615	+0.322	-0.819	-1.681
210	-1.462	-0.819	-0.494	+0.945	+1.432	+1.677	+0.605	-0.550	-1.624
200	-1.587	-1.063	-0.767	+0.687	+1.256	+1.687	+0.870	-0.264	-1.519
190	-1.664	-1.274	-1.016	+0.409	+1.040	+1.647	+1.108	+0.029	-1.367
180	-1.689	-1.447	-1.235	+0.118	+0.793	+1.554	+1.314	+0.322	-1.173
170	-1.664	-1.577	-1.416	-0.177	+0.522	+1.416	+1.478	+0.605	-0.945
160	-1.587	-1.658	-1.554	-0.466	+0.235	+1.235	+1.598	+0.870	-0.687
150	-1.462	-1.688	-1.647	-0.741	-0.059	+1.016	+1.669	+1.108	-0.409
140	-1.294	-1.669	-1.687	-0.994	-0.351	+0.767	+1.688	+1.314	-0.118
130	-1.086	-1.592	-1.677	-1.215	-0.633	+0.494	+1.658	+1.478	+0.177
120	-0.844	-1.478	-1.615	-1.400	-0.895	+0.206	+1.577	+1.598	+0.466
110	-0.578	-1.314	-1.505	-1.543	-1.130	-0.088	+1.447	+1.669	+0.741
100	-0.293	-1.108	-1.348	-1.639	-1.331	-0.380	+1.274	+1.688	+0.994
90	0	-0.870	-1.151	-1.684	-1.492	-0.661	+1.063	+1.658	+1.215
80	+0.293	-0.605	-0.920	-1.681	-1.606	-0.920	+0.819	+1.577	+1.400
70	+0.578	-0.322	-0.661	-1.624	-1.673	-1.151	+0.550	+1.447	+1.543
60	+0.844	-0.029	-0.380	-1.519	-1.687	-1.348	+0.264	+1.274	+1.639
50	+1.086	+0.264	-0.088	-1.367	-1.653	-1.505	-0.029	+1.063	+1.684
40	+1.294	+0.550	+0.206	-1.173	-1.566	-1.615	-0.322	+0.819	+1.68
30	+1.462	+0.819	+0.494	-0.945	-1.432	-1.677	-0.605	+0.550	+1.62
20	+1.587	+1.063	+0.767	-0.687	-1.256	-1.687	-0.870	+0.264	+1.51
10	+1.664	+1.274	+1.016	-0.409	-1.040	-1.647	-1.108	-0.029	+1.36

SECRET

TABLE 3.3

OPERATION Open Shot
SHOT DATE May 5, 1955
SHOT TYPE Nuclear
SHOT TIME 0510 (XXX) (POST)

RAYPAC

WEATHER DATA INPUT COMPUTATIONS

OPEN SHOT, TEAPOT

DATA TIME (XXX) (POST)	FCST	OBS
WIND		0525
TEMPERATURE		0525

HT Kft MSL	TEMP °C	WIND Deg/Kts		SOUND SPEED FPS	WIND COMPONENT HEADING				SOUND VELOCITY, V HEADING				V/V_B HEADING				HT GRD Kft	BRK HT Kft
					LSV	SGU	LND	TFH	LSV	SGU	LND	TFH	LSV	SGU	LND	TFH		
4.0	+ 3.9		0	1095.7	0	0	0	0	1095.7	→			1.0000	→			0	—
4.5	+15.3		0	1118.1	0	0	0	0	1118.1	→			1.0204	→			0.5	0
5.0	+14.6		0	1116.7	0	0	0	0	1116.7	→			1.0192	→			1.0	0.5
5.5	+15.1		0	1117.7	0	0	0	0	1117.7	→			1.0201	→			1.5	1.0
6.0	+15.0		0	1117.5	0	0	0	0	1117.5	→			1.0199	→			2.0	1.5
8	+10.1	130	8	1108.0	-13.4	-9.7	+ 4.2	+13.3	1094.6	1098.3	1112.0	1121.3	0.9990	1.0024	1.0149	1.0234	4	2.0
10	+ 4.9	150	14	1097.7	-23.0	-10.4	+14.2	+23.4	1074.7	1087.3	1111.9	1121.1	0.9808	0.9923	1.0148	1.0232	6	4
12	- 0.4	160	15	1087.2	-23.3	- 7.0	+18.5	+24.0	1063.9	1080.2	1105.7	1111.2	0.9710	0.9859	1.0091	1.0141	8	6
14	- 3.9	170	19	1080.2	-41.1	- 5.1	+41.1	+42.9	1039.1	1075.1	1121.3	1123.1	0.9483	0.9812	1.0234	1.0250	10	8
16	- 7.9	170	23	1072.2	-46.7	- 5.8	+46.7	+48.8	1025.5	1066.4	1118.9	1121.0	0.9359	0.9733	1.0212	1.0231	12	10
18	-12.4	180	29	1063.0	-36.8	+ 3.4	+45.1	+39.1	1027.2	1066.4	1108.1	1101.1	0.9375	0.9733	1.0113	1.0049	14	12
20	-19.0	180	31	1051.5	-38.3	+ 3.7	+48.2	+40.7	1013.2	1055.2	1099.7	1092.2	0.9247	0.9630	1.0037	0.9968	16	14
25	-29.7	190	33	1027.0	-23.4	+ 9.4	+37.8	+25.5	1003.6	1036.4	1064.9	1052.5	0.9159	0.9459	0.9719	0.9606	21	16
30	-40.9	210	28	1003.2	-11.4	+21.7	+38.2	+13.9	991.8	1024.9	1041.8	1017.1	0.9052	0.9354	0.9508	0.9283	26	21
35	-52.4	230	26	977.9	+ 2.3	+35.5	+39.1	+ 0.8	980.2	1013.4	1017.0	998.7	0.8946	0.9249	0.9282	0.9115	31	26
40	-61.1	220	29	958.6	- 6.0	+34.0	+46.3	+ 9.3	952.6	992.6	1005.4	967.9	0.8694	0.9059	0.9176	0.8834	36	31
45	-61.2	210	28	958.2	-13.8	+24.5	+46.0	+16.0	944.5	984.8	1005.2	975.2	0.8620	0.8988	0.9174	0.8900	41	36
50	-59.7	220	36	961.7	- 7.4	+42.2	+58.2	+11.6	954.3	1003.9	1019.9	973.3	0.8710	0.9162	0.9308	0.8883	46	41
55	-58.9	210	27	962.5	-13.3	+25.5	+45.3	+16.3	950.2	988.0	1008.8	978.8	0.8672	0.9026	0.9207	0.8942	51	46
60	-59.9	190	10	961.2	-10.2	+ 4.1	+16.6	+11.1	951.0	965.3	977.7	972.3	0.8679	0.8810	0.8923	0.8874	56	51
65																		
70																		
75																		
80																		

SANDIA CORPORATION
BLAST PREDICTION UNIT

SECRET

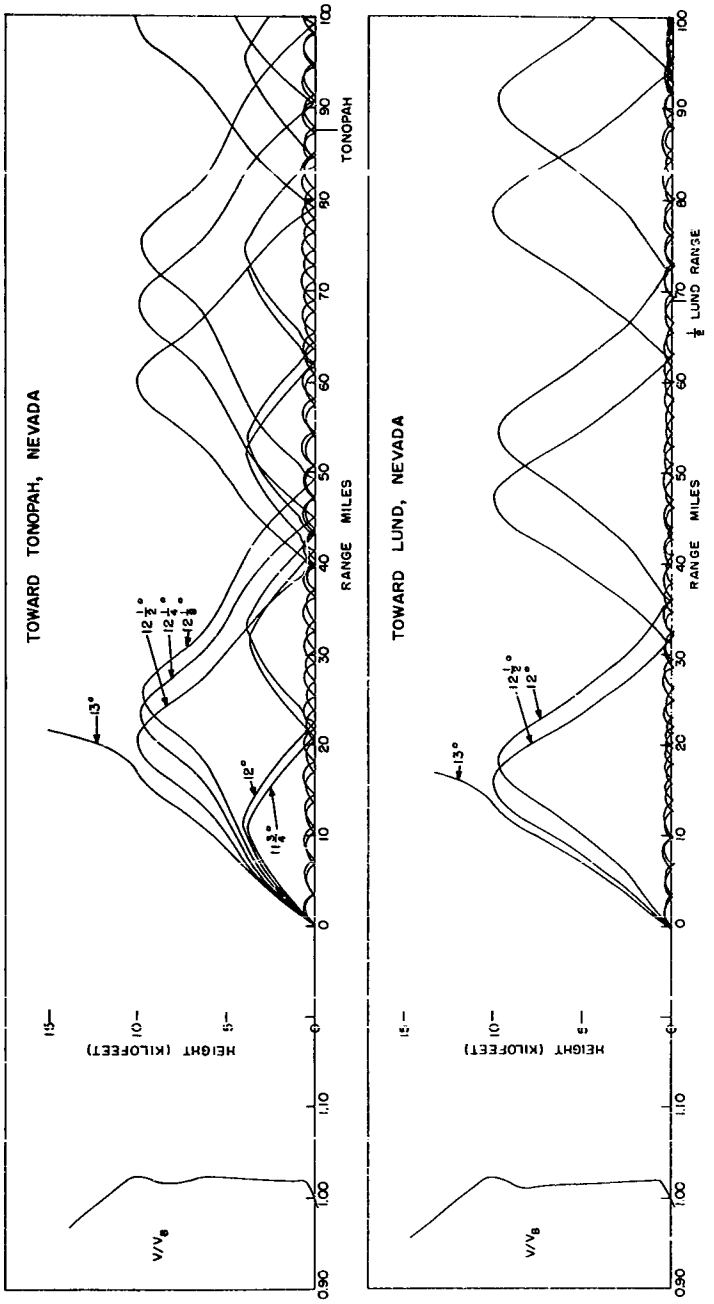

Fig. 3.7 -- Haypac Plots for Open Shot, Teapot

Combining Eqs 3.2 and 3.18 with the positive-phase duration (one-half the period determined by Eq 3.12), and both nearly doubling wave energy by reflection at R and diminishing its energy through each previous ground reflection by f, a relation is obtained that

$$P^2 = \frac{3(1+f)f^{n-1}}{(1.418)2\pi} \cdot \rho_o V_o^2 \cdot \frac{W^{2/3}}{R} \cot\theta_o \cdot \frac{\Delta\theta_o}{\Delta R} . \qquad (3.19)$$

Substitution of the previously determined value for ϵ, and the approximate relations $(1 + f) \approx 2$, $\rho_o \approx 10^{-3}$ g/cc, and $V_o \approx 1100$ fps (with necessary conversions for dimensional consistency), shows that overpressure,

$$P = 133\sqrt{\frac{W^{2/3} f^{n-1}}{R \tan\theta_o} \cdot \frac{\Delta\theta_o}{\Delta R}} \text{ mb} . \qquad (3.20)$$

In this relation, R and ΔR are expressed in miles, W in kilotons, nuclear yield, and θ_o in degrees. This equation is graphed, in Fig. 3.8, for W = 1 kt, n = 1, and R = 10 miles.

An overpressure computation is thus performed from measured $\Delta R/\Delta\theta_o$ and indicated θ_o at R on a Raypac ray plot. Figure 3.8 gives the overpressure for these values at the first ground strike, if at R = 10 miles. True overpressure may be scaled for observed R, number of reflections, and predicted weapon yield by

$$\text{true } P = (\text{graphic } P) \cdot \frac{W^{\frac{1}{3}} f^{\frac{n-1}{2}}}{(R/10)^{1/2}} \text{ mb} . \qquad (3.21)$$

Table 3.4 lists values for $f^{\frac{n-1}{2}}$ for integral values of n which might be found in practice.

TABLE 3.4

Reflection Factors Used in Blast Prediction*

n	$(0.60)^{\frac{n-1}{2}}$	$(0.75)^{\frac{n-1}{2}}$	$(0.936)^{\frac{n-1}{2}}$	$(0.997)^{\frac{n-1}{2}}$
1	1.0	1.0	1.0	1.0
2	0.775	0.866	0.967	0.999
3	0.600	0.750	0.936	0.997
4	0.465	0.650	0.906	0.996
5	0.360	0.563	0.876	0.994
6	0.279	0.487	0.847	0.993
7	0.216	0.422	0.820	0.991
8	0.167	0.365	0.793	0.990
9	0.130	0.317	0.767	0.988
10	0.100	0.275	0.742	0.987
11	0.0778	0.237	0.718	0.985
12	0.0602	0.206	0.695	0.984
13	0.0467	0.178	0.672	0.982
14	0.0361	0.155	0.650	0.981
15	0.0280	0.134	0.629	0.979
16	0.0217	0.116	0.609	0.978
17	0.0168	0.100	0.589	0.976
18	0.0130	0.0867	0.570	0.975
19	0.0101	0.0751	0.551	0.973
20	0.00781	0.0650	0.533	0.972

*$f^{\frac{n-1}{2}}$ (n is the number of cycles traversed through the atmosphere)

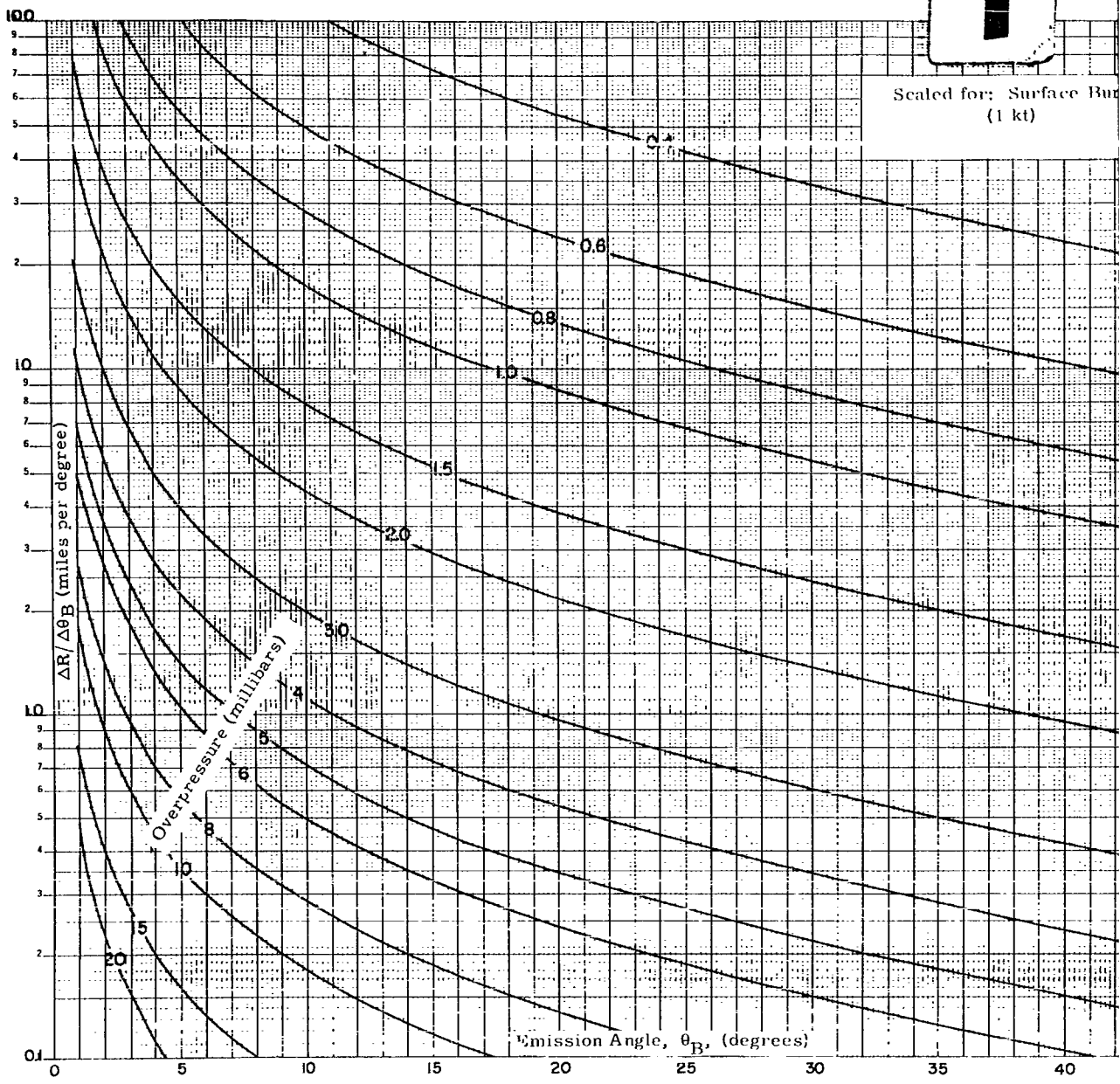

Fig. 3.8 -- Peak Overpressure Computation Chart

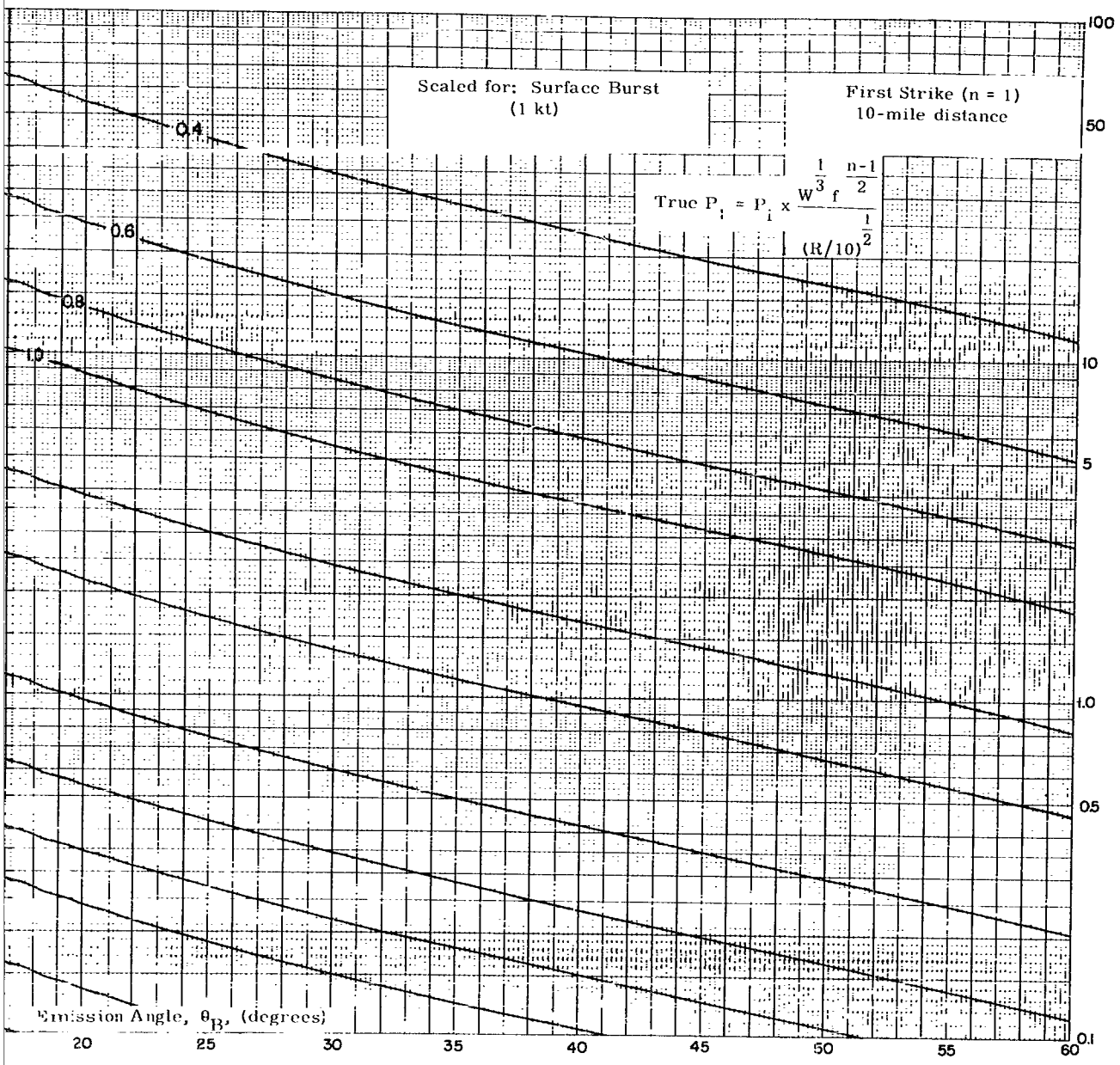

Fig. 3.8 -- Peak Overpressure Computation Chart

CHAPTER 4

VERIFICATION OF PREDICTIONS

4.1 ACCURACY OF PREDICTIONS PRIOR TO OPERATION TEAPOT[19]

The degree to which blast prediction, as used during 1951, 1952, and 1953 operations at NTS, was successful has been studied for the city of Las Vegas. Results are summarized in Table 4.1.

On the evening before each test, the USAF Air Weather Service issued a forecast for atmospheric conditions expected to exist at shot time.[20] Using these data—temperatures and winds as a function of altitude—as well as the predicted yield and burst altitude, the blast-prediction group computed the peak-to-peak blast pressures that would strike Las Vegas if the weather forecast and the predicted yield and burst altitude were true at shot time. These forecast pressures are listed in Table 4.1.

Predicted yield of the atomic device and a "scaling factor" equal to the square root of the yield ratio (nuclear-to-HE) were used to predict pressures from those observed on the HE shots fired at H-2 and H-1 hours before the test detonation (Table 4.1). While the weather forecast covers no more than the lower 50,000 feet of the atmosphere, HE shots and associated microbarograph measurements give information on shocks returned from the ozonosphere as well as the troposphere.

Only once, on Upshot-Knothole Shot 6, did the predicted pressures based on the previous evening's weather forecast call for damage (Table 4.1). However, this does not in any sense reflect the interesting situations that arise. For instance, on a number of occasions a sharp focus of blast was predicted a certain number of miles from the test site in the direction of Las Vegas; had this distance been close to a submultiple of the distance from the shot point to Las Vegas, this focus could have struck close to Las Vegas after a small number of reflections.

Moreover, although literal use of the weather-yield forecast might call for small or zero pressures in Las Vegas, a slight change from the forecast weather conditions could change pressures in Las Vegas tremendously.

Table 4.2 is an attempt to assign a "grade" to each of the two or three blast predictions for Las Vegas on each nuclear shot of Operations Buster-Jangle, Tumbler-Snapper, and

TABLE 4.1

Peak-to-Peak Blast Pressures in Las Vegas

Shot Series	Shot	Date	Predicted Yield (kt)	Measured RC Yield (kt)	Pressures in Las Vegas (ub)					Comments
					Troposphere			Ozonosphere		
					Predicted from previous night weather forecast	Predicted from -2 hour HE shot	Predicted from -1 hour HE shot	Measured	Predicted from -2 hour HE shot	Predicted from -1 hour shot	Measured	
Buster	A	10/22/51	0.2	2-5(x 10^{-3})	155	No shot	380	85	No shot	0	0	Yield much less than predicted
	B	10/28/51	8	3.8	375	No shot	0	10	No shot	80	130	Yield less than predicted
	C	10/30/51	15	15	585	No shot	0	5	No shot	70	130	Predicted focus absent at shot time
	D	11/ 1/51	25	21.5	0	No shot	>9000	>1100	No shot	0	0	Instrument off-scale
	E	11/ 5/51	35	30.5	0	No shot	2710	>765	No shot	0	0	Instrument off-scale
Jangle	S	11/19/51	1.3	1.1	0	No shot	0	0	No shot	45	25	
	U	11/29/51	1.3	1.2	215	230	No shot	30	20	No shot	15	
Tumbler-Snapper	1	4/ 1/52	1.3	1.1	100	75	40	300	0	15	0	
	2	4/15/52	1.3	1.05	0	0	0	30	0	40	0	
	3	4/22/52	25	30.0	0	50	0	0	0	500	1100	
	4	5/ 1/52	15-20	19.5	0	135-220	220-280	300	0	0	0	
	5	5/ 7/52	12	11.8	0	0	0	0	150	110	220	
	6	5/25/52	12	11.3	0	0	0	0	240	0	115	
	7	6/ 1/52	18	14.4	0	0	0	0	160	135	110	
	8	6/ 5/52	19	14.0	0	0	0	0	130	0	115	
Upshot-Knothole	1	3/17/53	15	16.2	160	1100	1220	360	0	0	0	Focus vanished during last hr
	2	3/24/53	35	24.5	280	0	0	0	370	500	380	
	3	3/31/53	1.5-2	0.30	250-325	100-140	0	130	0	0	0	
	4	4/ 6/53	11.6	11.0	0	1110	1020	>2320	0	0	0	Instrument off-scale
	5	4/11/53	0.4	0.22	190	230	230	420	0	0	2	
	6	4/18/53	20-40	23	2850-3520	No shot	0	330	No shot	0	0	
	7	4/25/53	35	43.4	250	625-860	0	285	50-70	215	280	
	8	5/ 8/53	30	26	1120	515	1780	550	250	0	0	Focus spread during last hr
	9	5/19/53	25	27	385	430	210	2380	0	75	185	Strong focus moved in during last hr
	10	5/25/53	14	14.9	0	0	0	125	0	0	335	
	11	6/ 4/53	63	60.8	0	0	0	0	0	0	180	

TABLE 4.2

Grade on Blast Prediction from Las Vegas

Shot	Prediction from Advanced Weather Forecast				Prediction from -2 Hour HE Shot				Prediction from -. Hour HE Shot			
	Good	Fair	Poor	Bad	Good	Fair	Poor	Bad	Good	Fair	Poor	Bad
Buster-Able		X								X		
Baker		X							X			
Charlie			X						X			
Dog				X						X		
Easy				X						X		
Jangle-Surface	X								X			
Underground		X				X						
Turobler-Snapper-1		X				X				X		
2	X				X				X			
3		X			X				X			
4		X			X				X			
5	X				X				X			
6	X				X				X			
7	X				X				X			
8	X				X				X			
Upshot-Knothole-1		X					X				‹	
2	X				X				X			
3	X				X				X			
4				X	X				X			
5			X						X			
6				X		X				X		
7	X					X				X		
8			X		X						::	
9				X				X				X
10	X				X				X			
11	X	—	—	—	X	—	—	—	X	—	--	—
Total	11	7	3	5	13	4	1	1	16	6	2	1
					(No data for 7 shots)				(No data for shot)			

SECRET

Upshot-Knothole. Weather in Nevada was remarkably stable during the Tumbler-Snapper series, and blast predictions based on weather forecasts of the previous evening were all fair or good. On Buster-Jangle and Upshot-Knothole, because the weather was variable, essentially half of the advance blast forecasts were fair or good, half poor or bad. An average for 26 shots, on which blast predictions were based solely on the weather forecasts of the previous evening, was 69 per cent fair or good, 31 per cent poor or bad.

Predictions based on scaling of data from the high-explosives shots were remarkably good for both Buster-Jangle and Tumbler-Snapper. In three instances (Upshot-Knothole Shots 1, 8, and 9), weather changes in the final hour before the nuclear shot caused considerable embarrassment to the blast-prediction group. On two of these occasions the H-1-hour predictions called for near-damaging blast to strike Las Vegas; the actual blast pressure was anything but damaging. On another occasion (Upshot-Knothole Shot 9), there was no prior indication that damaging blast would strike Las Vegas, but recorded pressures from the nuclear shot were very near damaging. Thus, although the record for predictions from the H-1-hour shot stands at 88 per cent fair or good, 12 per cent poor or bad, "The evil that men do lives after them; the good is oft interred with their bones."

Microbarograph measurements on high-explosives shots at H-2 and H-1 hours have an outstanding advantage in that they alone supply a means of predicting blast refraction to earth from the ozonosphere. But they also have an outstanding weakness as far as both troposphere and ozonosphere shocks are concerned; they come close to being "yes-no"-type tests. When there is a blast focus, microbarograph measurements by a small number of instruments at preselected locations cannot tell us the extent of the focal "point"; worse, they cannot say how near the city the focus may be. To improve accuracy in forecasting blast pressures transmitted through the troposphere, we need improved weather forecasts.

4.2 VERIFICATION OF TEAPOT PREDICTIONS

A summary of predictions actually presented at Teapot briefings has not been made because the main source of inaccuracy in these calculations was in the weather forecast. Consequently, to check objectively the actual blast-prediction system, shot-time weather records have been used to provide after-the-fact pressure-wave amplitude estimates for each microbarograph recording site.

Signal amplitudes expected to propagate under surface inversions were estimated from the limiting equations presented in Section 3.2. A scatter diagram of computed versus observed overpressures from Eq 3.10 is shown in Fig. 4.1, and from Eq 3.11 is shown in Fig. 4.2. From this comparison it appears that Eq 3.10 is satisfactory for nuclear shots,

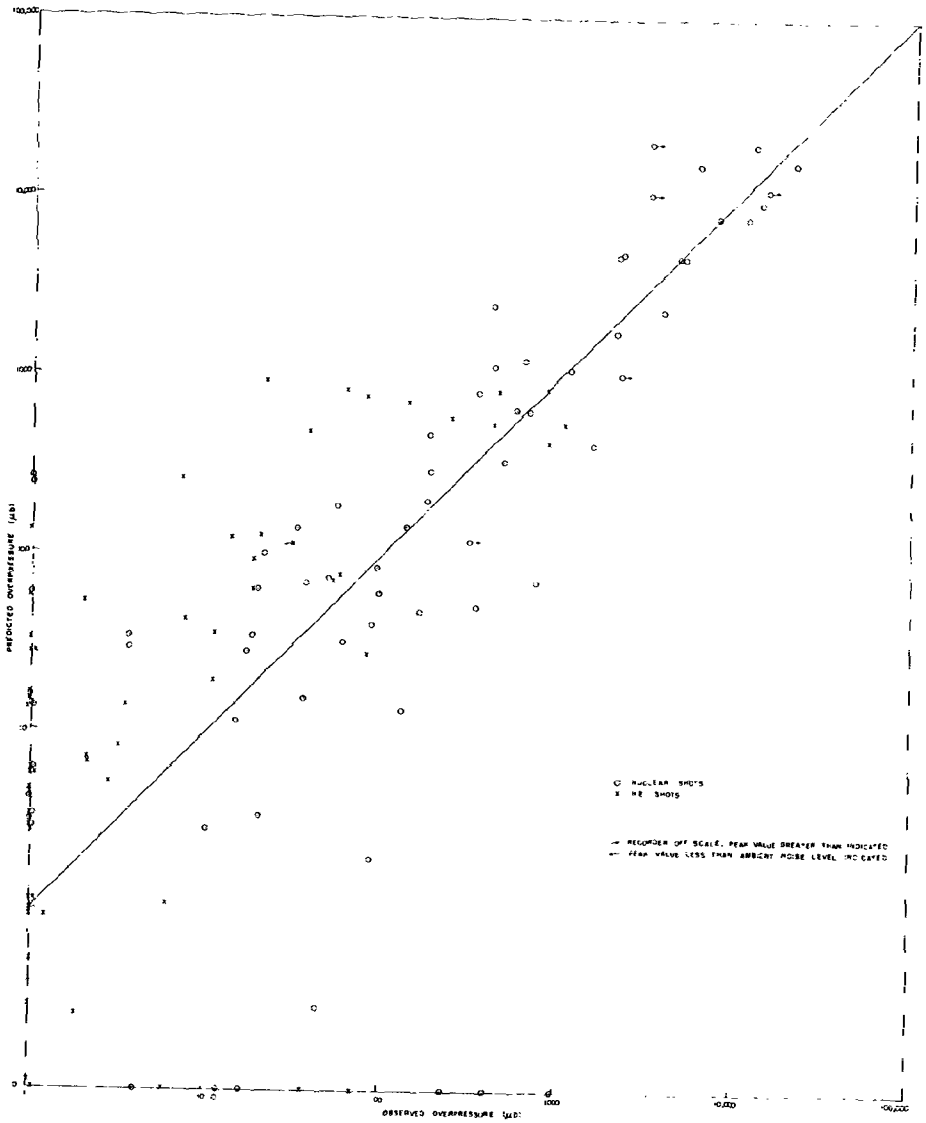

Fig. 4.1 -- Verification of Inversion-ducted Overpressures Predicted from Eq 3.10, Teapot

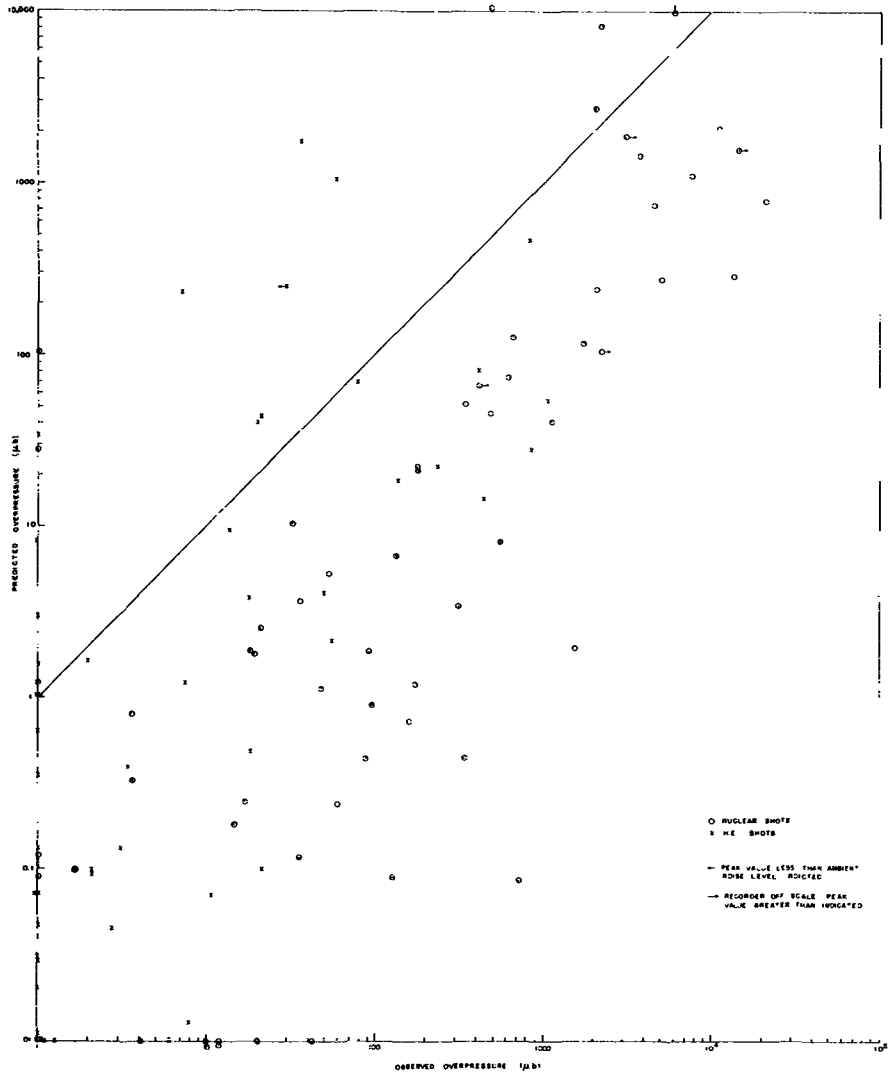

Fig. 4.2 -- Verification of Inversion-ducted Overpressures Predicted from Eq 3.11, Teapot

but generally overestimates pressures from HE preliminary blasts. On the other hand, Eq 3.11 generally underestimates overpressures except in a few of the HE cases. Equation 3.11 would probably be improved by using f = 0.75, as used in Eq 3.10. Scatter in verification is still not altogether satisfactory, and it is difficult to convince test site personnel that the Blast Prediction Unit verified much better at a range of 100 miles than of 10 miles. Since signal ducts under an inversion give signal intensities which decrease rapidly with distance, no damaging conditions would be forecast for or observed at surrounding cities from this type of signal propagation, so prediction errors observed within NTS would never have serious consequences outside.

Verification of predictions for complex atmospheres has also been computed for Operation Teapot. Where foci appear, large gradients of overpressure with distance would be predicted, although sufficient observations have never been obtained actually showing such narrow intense sound bands as theory indicates. Thus, a large error in predicting overpressure could have been a small error in predicting focal distance. This factor has been considered by forecasting a range of overpressures for distances within 5 miles of the recording site. These ranges are plotted against observed overpressures in Fig. 4.3. Most cases verified showed quiet zones falling within 5 miles of the recorder, and this is indicated by a dashed extension down from the range line. A similar verification, but for distances within 10 miles, increased the computed ranges only slightly and allowed sound at the three stations otherwise predicted to have silence. It appears that verification is about as good as could be hoped for. A further check of complex cases was prepared, comparing observed overpressures with prediction scaled from H-1-hour HE preliminary shots. Results for both $W^{1/3}$ and $W^{1/2}$ scaling are shown in Fig. 4.4. According to Eq 3.19, overpressures should be proportional to $W^{1/3}$. Yet it appears that $W^{1/2}$ proportionality more nearly represents the true condition. Under a given atmospheric condition, the probability of constructive interference increases with increased yield, since the positive-phase duration is increased. Thus, $W^{1/3}$ scaling would provide a minimum estimate of larger yield effects, and $W^{1/2}$ scaling includes empirically the additive effects of interference. Probably a better scaled prediction could be made if the number of cycles of signal observed from the HE in one positive-phase duration period for the atom test were multiplied by the $W^{1/3}$ scaled amplitude.

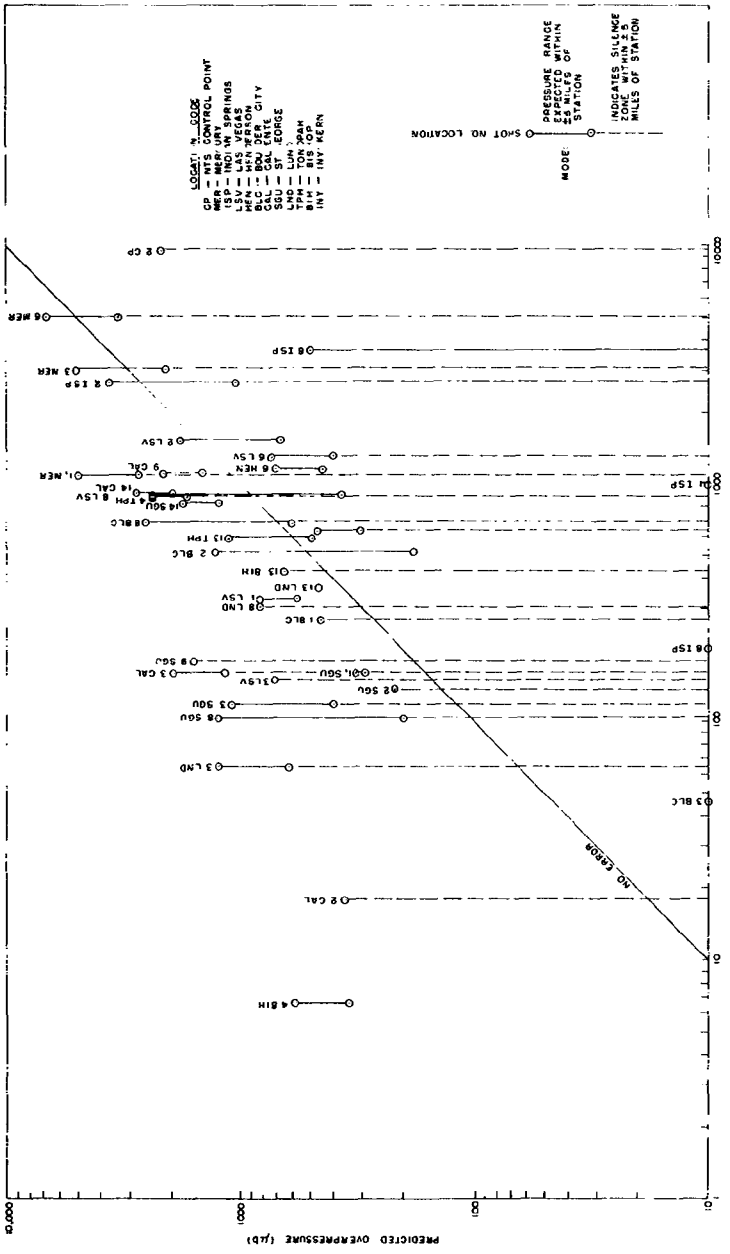

Fig. 4.3 -- Verification of Raypac-predicted Overpressures, Teapot

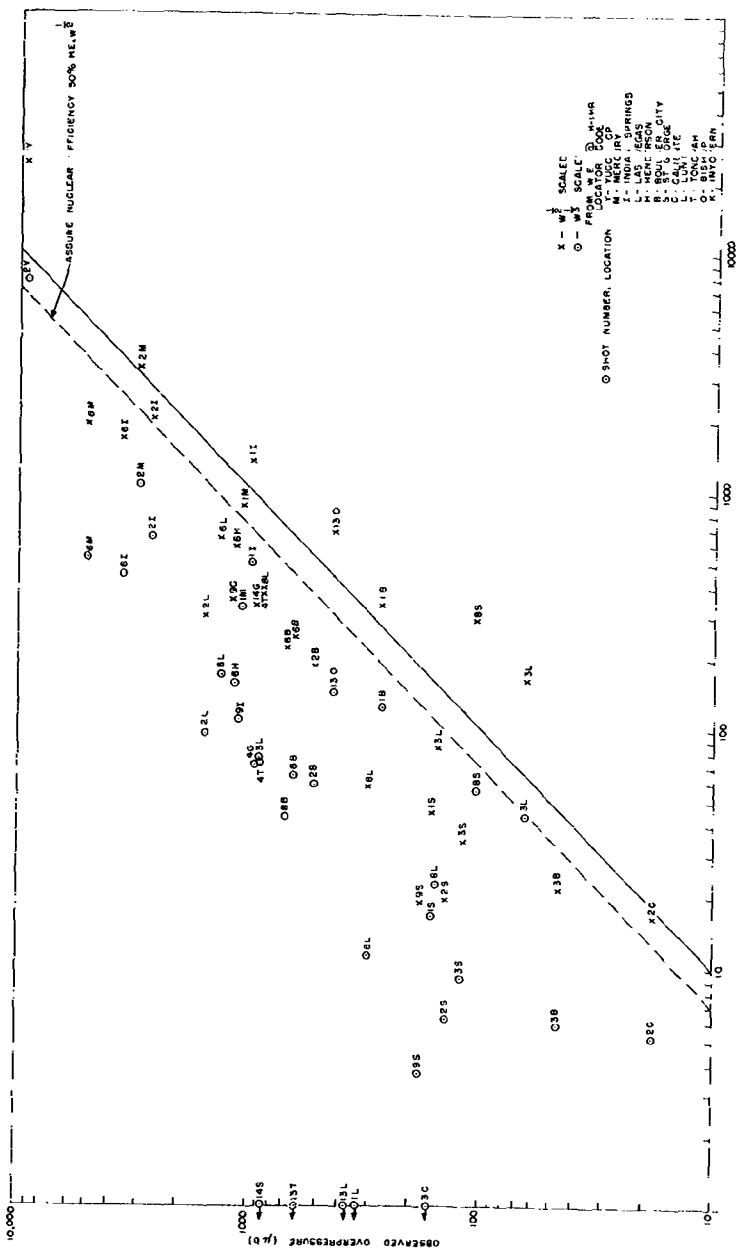

Fig. 4.4 -- Verification of HE-scaled Overpressures, Teapot

Ozonosphere signals are generally observed 30 to 60 seconds after troposphere signals, so they are easy to recognize on recordings. Thus, a separate verification of HE-scaled ozonosphere signals was made as shown in Fig. 4.5, using $W^{1/3}$ scaling, and in Fig. 4.6, using $W^{1/2}$ scaling. Again the $W^{1/2}$ scaling appears to give the best results, but the relative improvement over $W^{1/3}$ scaling is less than for complex tropospheric conditions.

It is likely that errors in prediction either from computation or scaling could be explained qualitatively by consideration of time and space variations of the weather.

4.3 ACCURACY OF WEATHER PREDICTIONS

A summary of vector errors in predicting velocity of sound in the southeast direction for the evening briefing has been prepared for the 1951, 1952, and 1953 series of tests. In Fig. 4.7, average and standard errors are plotted against altitude, MSL. Most of these errors result from inaccuracy of wind prediction. Mean errors and magnitudes of errors in speed of sound, a function of temperature, are plotted against altitude in Fig. 4.8. Temperature forecast errors are relatively small, but it is noticeable that velocity errors are comparatively large; so large, in fact, that a detailed pattern for sound propagation, derived from forecast data, may be changed considerably. However, prediction errors are not disproportionate when compared with errors which would result from assuming that 0100 PST upper-air observations persisted until shot time. Standard error for all point-level forecasts is ±26 fps, whereas that for 0100 PST data persistence is ±18 fps. Assuming persistence of the atmosphere for even 1-hour periods gives errors in sound propagation intensity which are occasionally large, as may be noted by comparing the E-2-hour and H-1-hour HE predictions in Table 4.1. In particular, note Upshot-Knothole Shots 3, 6, 8, and 9.

Hourly variability of the wind at any level less than 30,000 feet MSL has a standard deviation near ±6 fps.[21] It is believed that at altitudes greater than 30,000 feet and in jet stream regions this variability becomes much larger.[22] The Meteorology Section of Sandia Corporation's Field Test Organization operated Project Rawijet to measure this high-level variability, but the necessary statistical analysis is not yet complete. At present, it seems reasonable to conclude that prediction of blast-pressure patterns and magnitudes will be subject to frequent errors in verification whether based on weather forecasts or on pretest HE shot results.

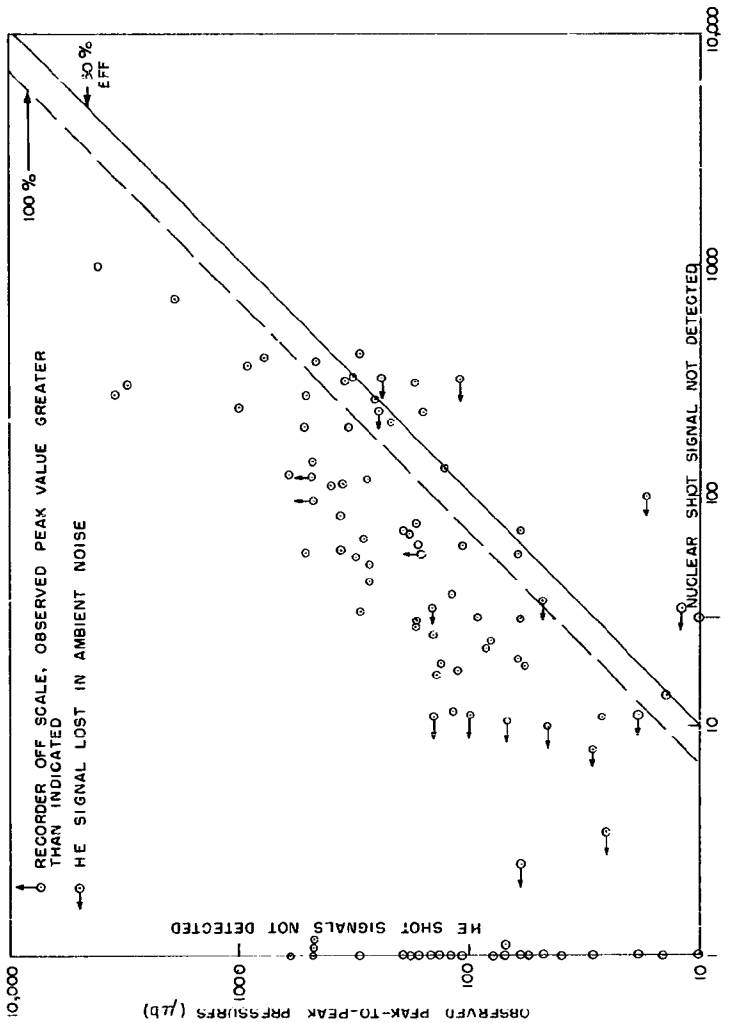

Fig. 4.5 -- Verification of $W^{1/3}$ Scaled HE Overpressures, Teapot

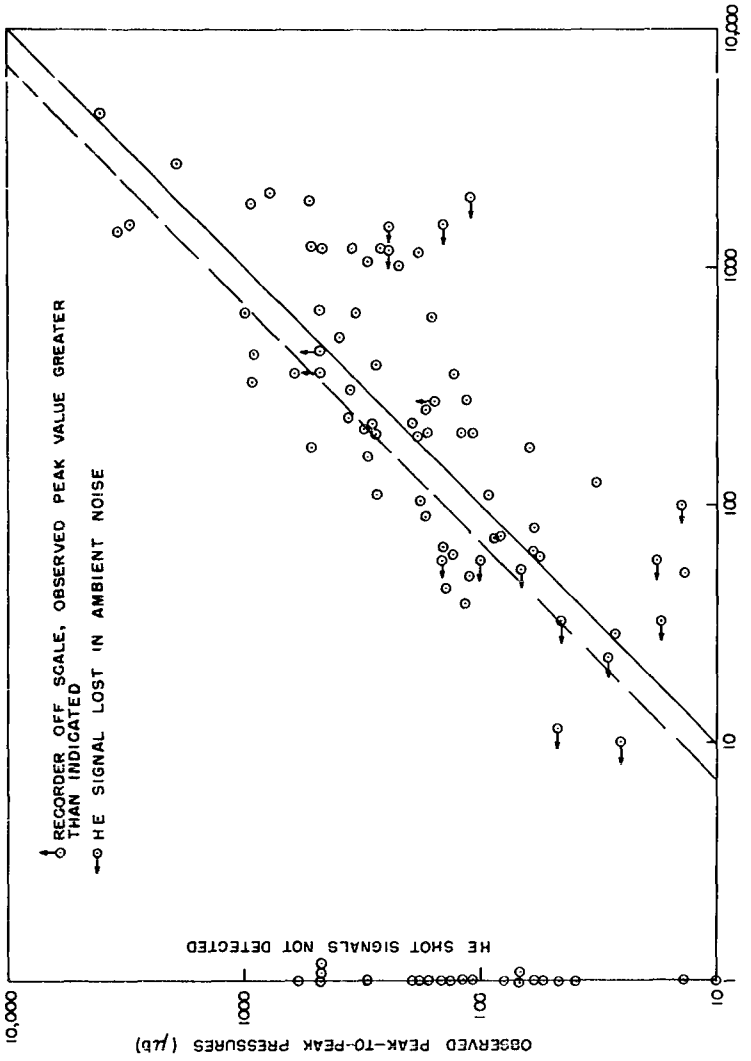

Fig. 4.6 -- Verification of $W^{1/2}$ Scaled HE Overpressures, Teapot

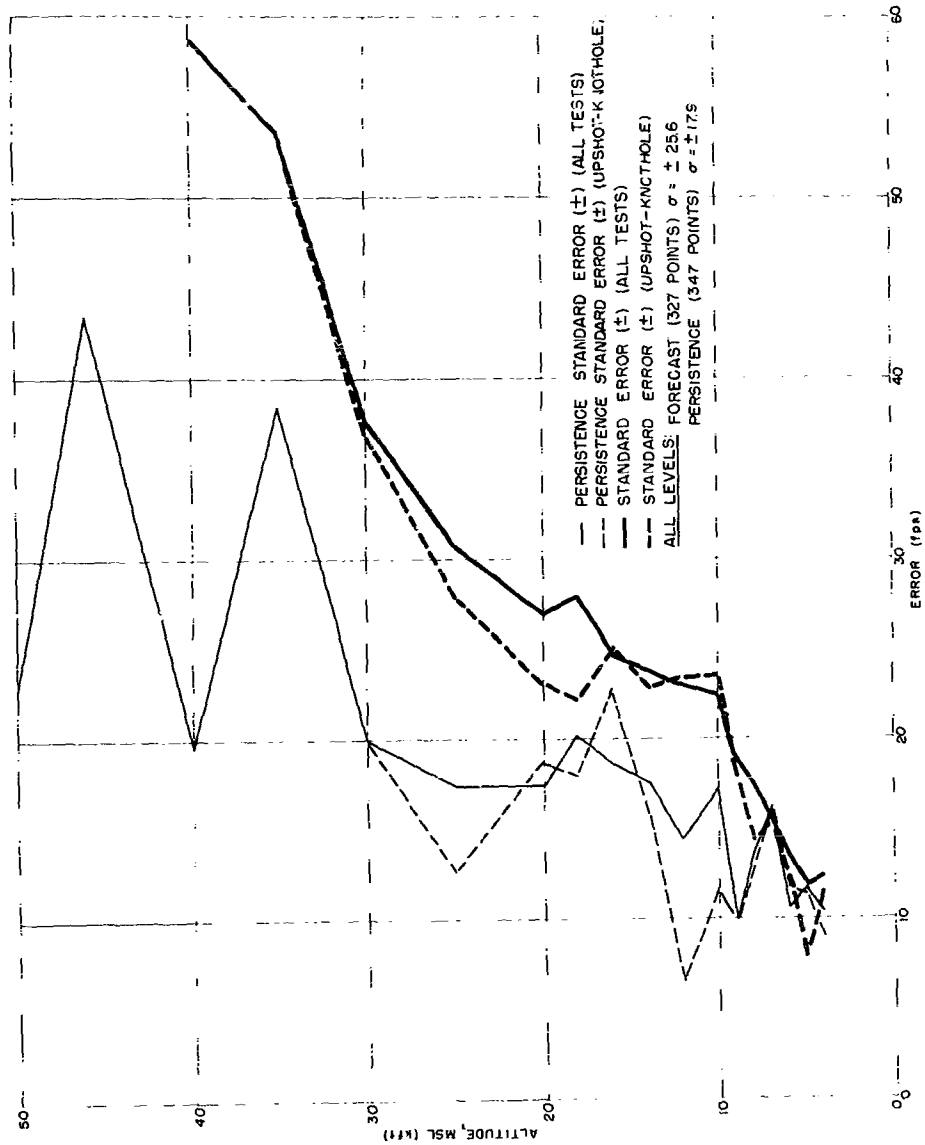

Fig. 4.7 -- Errors in Predicting Sound Velocity, Upshot-Knothole

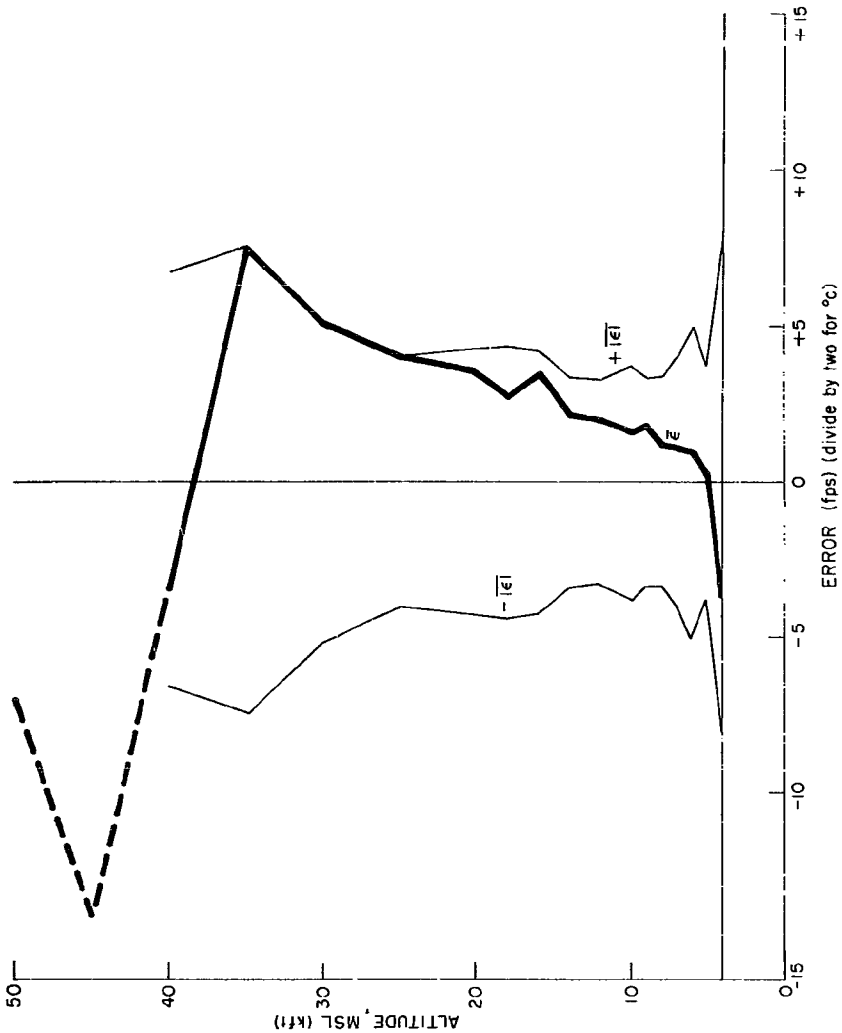

Fig. 4.8 -- Errors in Predicting Sound Speed, Upshot-Knothole

As might be expected, errors in predicted winds are not randomly variable with successive heights. For the three test series, mean thickness of atmospheric layers having errors of the same sign was found to be 6000 feet. The mean error within such layers was 16 fps (Fig. 4.9). From these values, general classes of likely sound-propagation patterns may be derived from a meteorological-forecast condition. However, application as shown

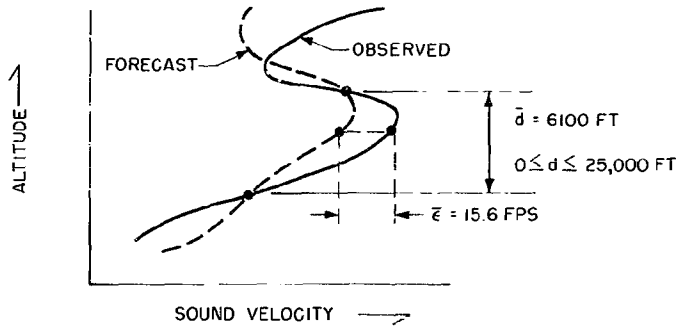

Fig. 4.9 -- Layer Character of Errors in Predicting Sound Velocity

in Fig. 4.10 emphasizes the fact that adding possible errors to any forecast structure may change sound intensity expected at a point location from zero to many times the level predicted by literal application of the forecast sound velocity-height relation.

To summarize, more accurate wind forecasts would be helpful in predicting shock intensities for inhabited localities around the NTS, but even forecasts as reliable as 1-hour persistence could conceivably allow amplitude prediction errors large enough to cover the range from insignificance to damage near focal points.

A theoretically developed function relating the probability of damaging shocks to atmospheric structure has been suggested, but the complexity of the sound path and energy equations has discouraged the attempt thus far. On the other hand, as more data on these relations accumulate, an empirical function may be found that will work reasonably well.

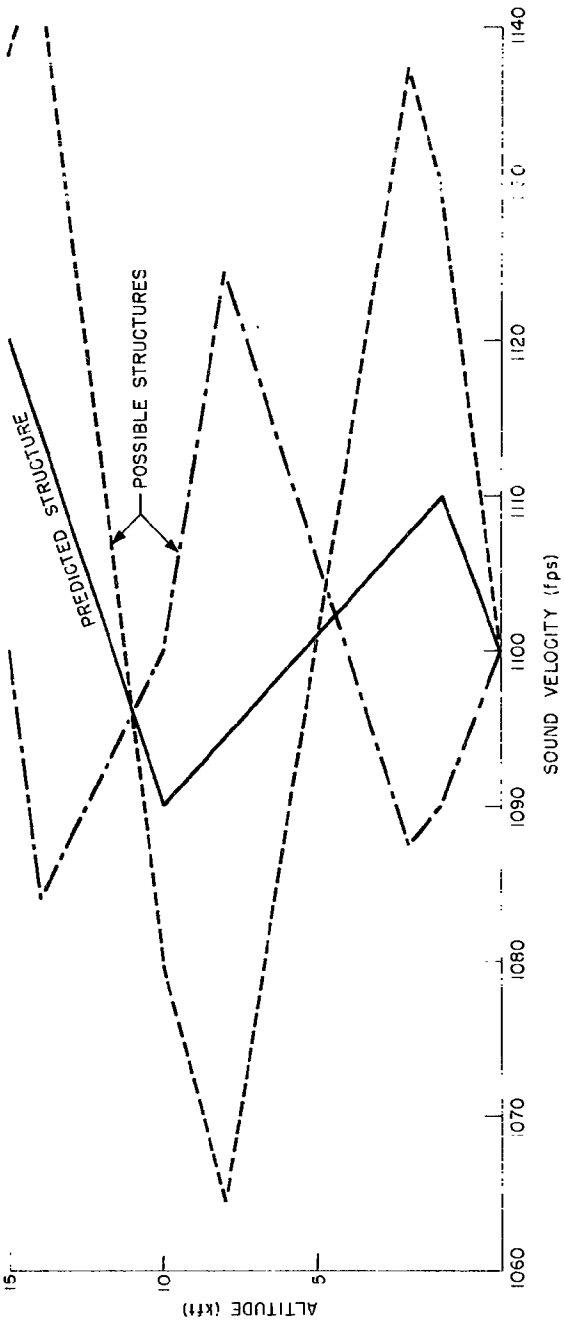

Fig. 4.10 -- Possible Sound Velocity Structures Caused by Forecasting Errors

CHAPTER 5

HIGH-ATMOSPHERE (OZONOSPHERE, IONOSPHERE) SIGNALS

5.1 DEDUCING OZONOSPHERE WEATHER CONDITIONS

Although we have distinct evidence[1] that sound signals from nuclear explosions do, under certain circumstances, travel at least part of their paths to remote distances through the higher-level atmospheric regions known as the ozonosphere and ionosphere, established meteorological procedures do not as yet permit us to make measurements in these regions. However, Johnson[23] and Crary[24] have described methods for deducing atmospheric conditions at these higher levels from distances, arrival times, and characteristic velocities of sounds measured at three or more azimuths from a shot point.

In an attempt to measure the characteristic velocities of some of the "anomalous" signals that had been returned from the ozonosphere and ionosphere, dual microbarograph stations were operated at several outlying locations (Fig. 2.6) during the Upshot-Knothole series of nuclear test shots. The characteristic velocity of a signal, which represents the velocity of sound at the level where the ray became horizontal, is the apparent velocity of travel between the dual stations (Fig. 5.1). (If the two stations are at different elevations, minor modifications in the computation procedure outlined below are necessary.)

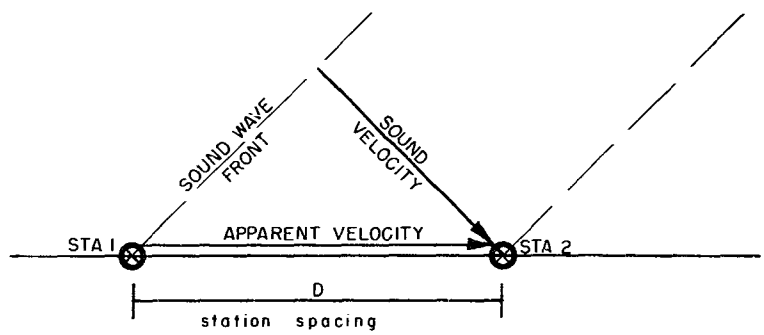

Fig. 5.1 -- Geometry of Dual Microbarograph Sound Recording

Cox et al[3] have given the distance traveled by a signal through the lower atmospheric levels (in which measurement is possible) as

$$D_m = 2 \sum_{i=0}^{i=m-1} \left(\frac{h_{i+1} - h_i}{V_{i+1} - V_i} \right) \left(\sqrt{V_p^2 - V_i^2} - \sqrt{V_p^2 - V_{i+1}^2} \right). \tag{5.1}$$

The time required for this travel is

$$T_m = \sum_{i=0}^{i=m-1} \left(\frac{h_{i+1} - h_i}{V_{i+1} - V_i} \right) \log \left[\frac{V_p + \sqrt{V_p^2 - V_i^2}}{V_p - \sqrt{V_p^2 - V_i^2}} \cdot \frac{V_p - \sqrt{V_p^2 - V_{i+1}^2}}{V_p^2 + \sqrt{V_p^2 - V_{i+1}^2}} \right]. \tag{5.2}$$

(Values to the maximum meteorologically observed level are denoted by m.) Subtracting these values of D_m and T_m from the total recorded distance and time traveled by a given signal gives D' and T', the distance and time of travel in the unknown atmosphere.

Various postulations have been made concerning atmospheric structures that satisfy these conditions.[23-30] In general, it has been found that differences in the postulated intermediate structures do not appreciably change the estimated heights at which the rays become horizontal.[29]

For convenience, the unknown region was taken to extend from that altitude at which meteorological observations stopped to that where the velocity of sound was equal to V_p. An evaluation procedure which assumed this region to consist of two layers, each having linear velocity-altitude gradients, could be used to determine a family of solutions satisfying the (T', D', V_p) conditions (Fig. 5.2). When θ is taken to be the inclination angle of the ray in question to the horizontal ($V/\cos\theta = V_p$), the family of solutions may be described by the following relations.[23] (The primes and double primes indicate the two limiting structures of the family; $gd^{-1}\theta$ is the anti-Gudermanian of θ.)

$$\sin\theta' = (D'/T'V_p)\, gd^{-1}\theta', \tag{5.3}$$

$$V' = V_p \cos\theta', \tag{5.4}$$

$$h' = D' (1 - \cos\theta')/\sin\theta'. \tag{5.5}$$

$$\sin\theta'' = \sin\theta_m + (D'/T'V_p)(gd^{-1}\theta'' - gd^{-1}\theta_m), \tag{5.6}$$

$$V'' = V_p \cos\theta, \tag{5.7}$$

$$h'' = (V'' - V_m)\, T'/2(gd^{-1}\theta_m - gd^{-1}\theta''). \tag{5.8}$$

The points at which changes in the intermediate gradients take place describe an approximately straight line, dashed from (h_m, V') to (h'', V'') in Fig. 5.2, for all solutions of a family.

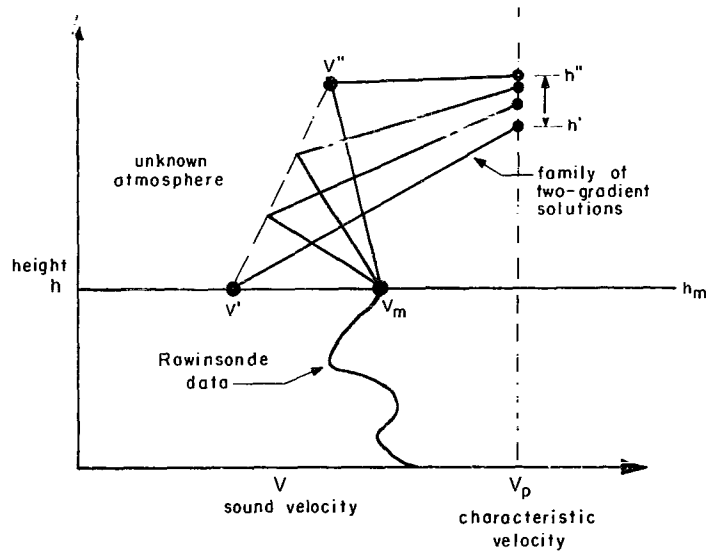

Fig. 5.2 -- Two-gradient Solutions of Upper Atmosphere Sound Velocity

If the earliest signal of an ozonosphere set is used to determine a family, succeeding signals having higher characteristic velocities may, in turn, be evaluated, using as new values of h_m, V_m, T_m, and D_m the range of values just determined. While this method has been used successfully by other investigators dealing with smaller numbers of weaker signals, on nuclear tests as many as 25-30 distinct ozonosphere return pulses may be received over a period as long as 100 seconds. Successive application of the two-gradient solution was found to give reasonable intermediate conditions for only two or three successive signals. Further successive solutions would have entailed zero or negative sound velocities in intermediate regions, an obvious impossibility. Determination of a multiple-parameter structure that could be evaluated as an approximation toward satisfying a complete set of data would indeed be a formidable task. Consequently, only the strongest signal in each set was evaluated by use of the two-gradient method, the mean value of h' and h" being taken as the height of the ray crest. However, successive solutions were used to compute crest heights for ionosphere

returns arriving considerably later than those of the ozonosphere set; here the two-gradient intermediate conditions appeared reasonable.

Results of this analysis of the Upshot-Knothole data are plotted in Fig. 5.3. Examination of the grouping of points by stations led to the discovery that, when plotted as D/V_pT vs h/D, these points fell very nearly on a straight line even when the four ionosphere signals were included (Fig. 5.4). The RMS line computed for these variables is

$$h/D = 0.865 - 0.789\ D/V_pT\ . \qquad (5.9)$$

When h, the height of the crest, is computed from Eq 5.9 without regard for known meteorological conditions or the azimuth from the shot point, computed crest heights vary only by the amounts indicated by the vertical line segments in Fig. 5.3. In several instances, these changes were small enough to be negligible on the scale of this plot; in nearly every instance, the change was less than $h'' - h'$, the range of uncertainty for the two-gradient solution. No analytical proof for the validity of this simplified empirical relation has yet been developed.

A check was made of the generality of Eq 5.9, for height finding, by computing ray paths and arrival times for signals traveling a broad range of possible atmospheric structures. The various structures used for the check computation are shown in Fig. 5.5. In Fig. 5.6, computed parameters are plotted with the line described by Eq 5.9 for comparison. These points fall below the Upshot-Knothole data line because the irregularities of a true atmospheric structure have been smoothed out with lines in Fig. 5.5. This serves to increase $\overline{V}$ and so decrease h/D below a true value for atmospheric transmission. Thus, the approximation is entirely adequate for height finding and may be used to replace laborious solution methods which have been previously derived,[23, 26, 29] with no loss of accuracy.

5.2 OBSERVATIONS FROM OPERATION UPSHOT-KNOTHOLE

Values of T and V_p for all anomalous signals strong enough to be identified on both recordings from a dual station were then determined from microbarograph records. Altitude-velocity points for individual observations were computed from Eq 5.9 and plotted in Figs. 5.7 and 5.8. All points have been coded in accordance with the relative peak-to-peak pressures of the signals and weighting factors assigned to each amplitude, A, range. The speed-of-sound curve adopted by the Rocket Panel[31] has been superimposed on each plot for reference, as have the observed meteorological data for lower atmospheric levels obtained by the Air Weather Service.[20]

About 60 points were plotted for each of three altitude levels: 80-120 kft (Zone I), 120-140 kft (Zone II), and 140-180 kft (Zone III). Thus, enough data points were obtained to

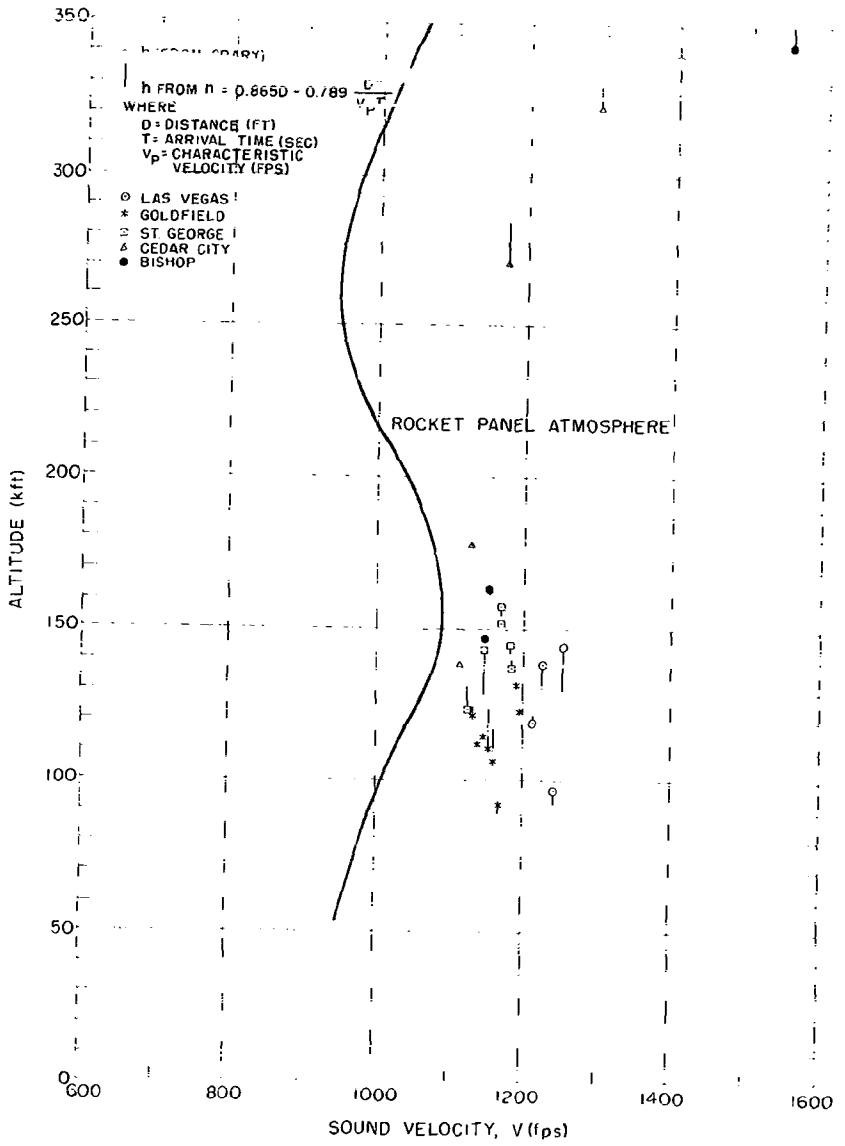

Fig. 5.3 -- Upper Air Sound Velocities from Upshot-Knothole Microbarograph Recordings

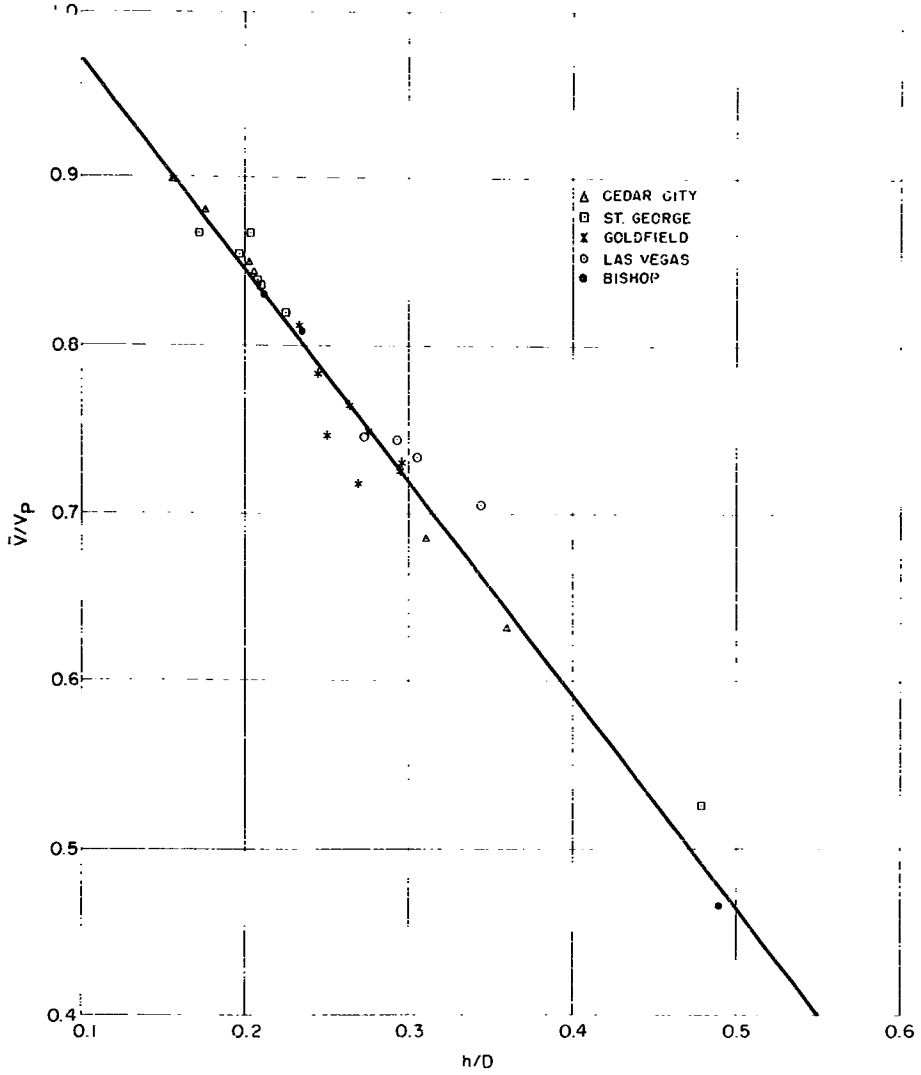

Fig. 5.4 -- Linearized Solution for Upper Air Sound Velocities, Upshot-Knothole

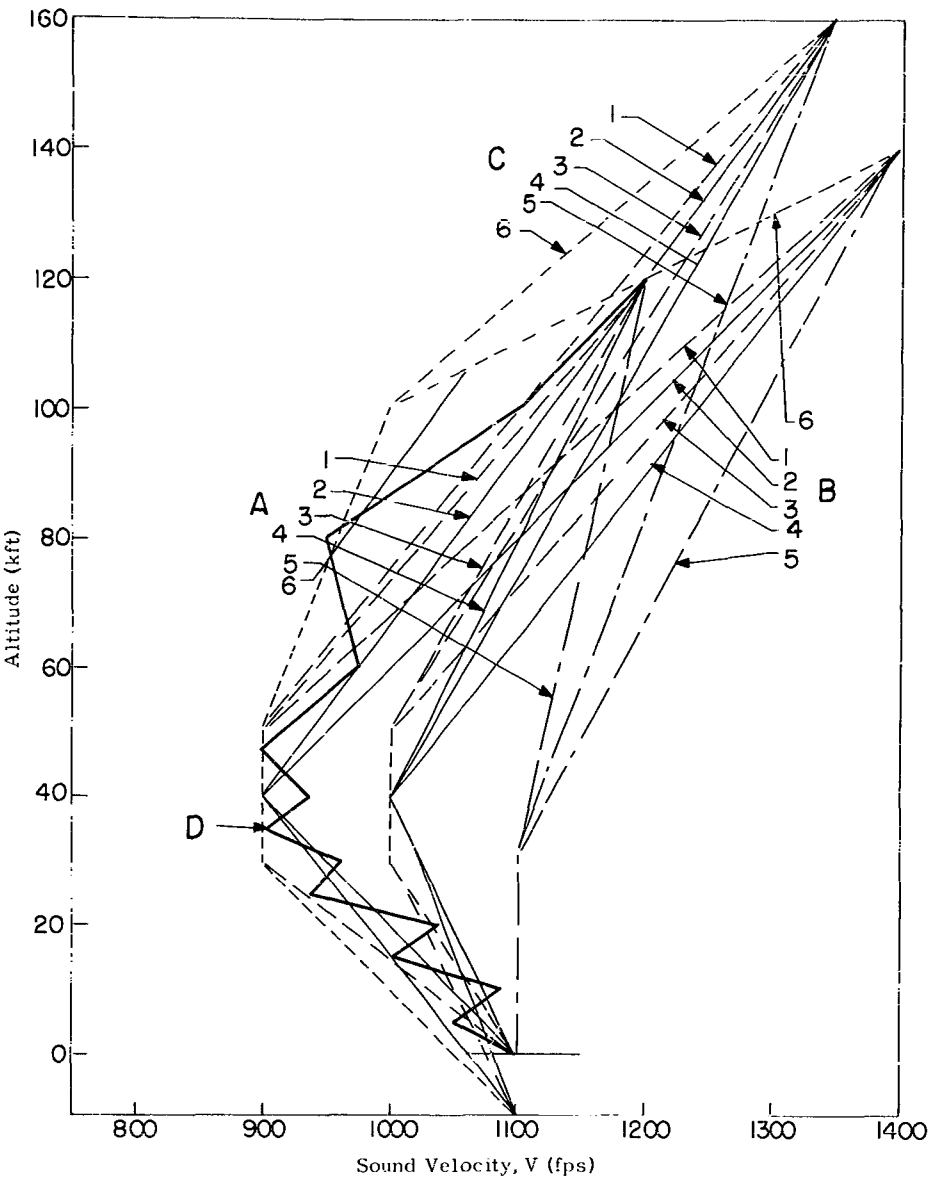

Fig. 5.5 -- Atmospheric Sound Velocity-Altitude Structures Used in Checking Empiric Height Equation

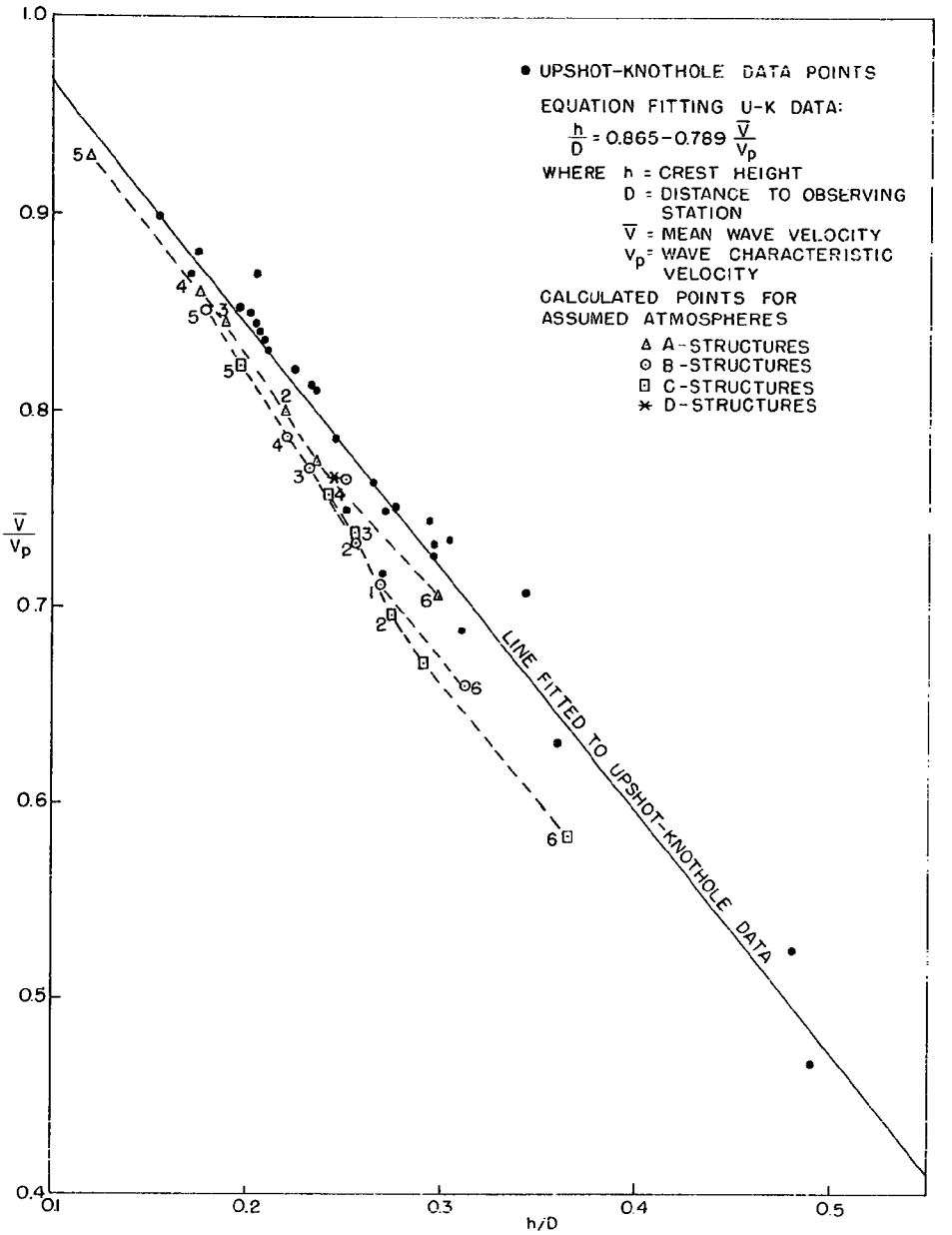

Fig. 5.6 -- Computed Sound Travel Parameters from Assumed Atmospheric Structures

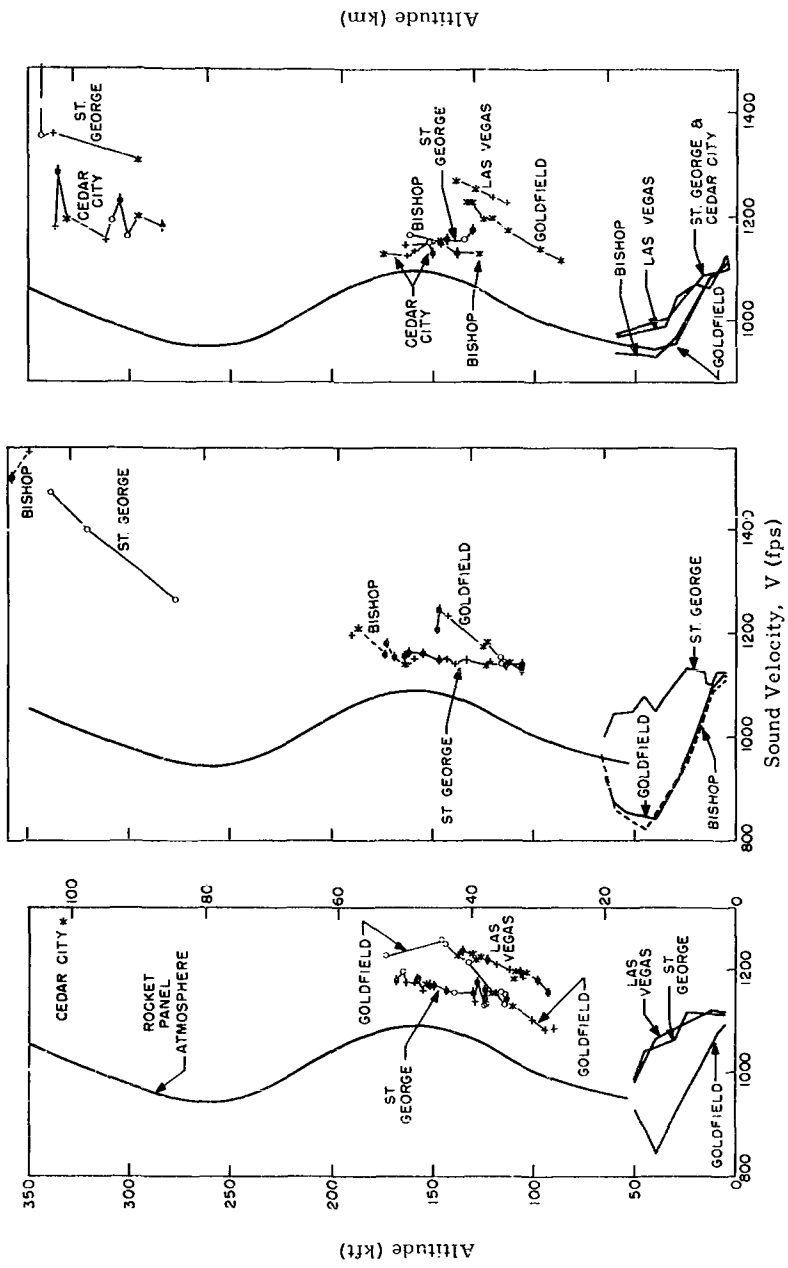

Fig. 5.8 -- Ozonosphere and Ionosphere Sound Velocities, Upshot-Knothole

permit a statistical evaluation for the ozonosphere region, and the weighting factors were applied to determine a mean value of V for each altitude range at each station. No attempt has been made here to evaluate the meager ionosphere data statistically.

If sound and wind speeds are directly additive, as has been assumed, these parameters may be separated when measurements at three or more azimuths are obtained. For Zones I and II, mean values of V were found for only three stations, Las Vegas, Goldfield, and St. George, and the sound and wind speeds could be separated directly. For Zone III, data points were obtained for five stations and an RMS fitted solution was possible. Strictly speaking, the relative amplitude weighting procedure for a given azimuth should take into account the differences in yield for different shots; for simplicity, however, the mean values of V were weighted in accordance with the number of records contributing to the mean. These mean values of V are plotted against azimuth in Fig. 5.9, as are the direction cosine curves and the separated mean wind and sound speeds. In Fig. 5.10, the three mean sound speeds are compared with the Rocket Panel Atmosphere,[31] the NACA Atmosphere,[32] and Cox's Helgoland data.[27]

These data indicate temperatures in the ozonosphere region to be about 60°C higher than those estimated in the Rocket Panel Atmosphere and more in line with earlier NACA data. However, the deviation may be attributable to the peculiar geographic location, to marked variations from normal of the entire atmosphere during this test period, or to correlation with specific atmospheric patterns required for safe nuclear testing.

Actually, the data used in this analysis represent probably no more than half the anomalous signals received at the six dual stations during Upshot-Knothole. Some dual stations were not operated during several test shots, and equipment failure and procedural uncertainties took further toll of potentially usable data. Nevertheless, the experience gained on this operation established greater confidence that significant results were possible from this type of instrumentation, so later tests could be instrumented with much greater efficiency.

5.3 OBSERVATIONS FROM OPERATION CASTLE

Microbarograph operations for Castle were begun before Upshot-Knothole data on the ozonosphere had been analyzed. Thus, instrumentation was not set up to give optimum results. In fact, inadequate time synchronization of the various records at an absolute minimum number (3) of distant recording stations, shown in Fig. 2.8, made resolution of signal data into temperature and wind observations impossible for most shots. The great distance to the Ponape recording site made the exact number of reflected cycles traversed through the atmosphere indeterminate. From 2 to 5 cycles seemed to be required for most signals, but the

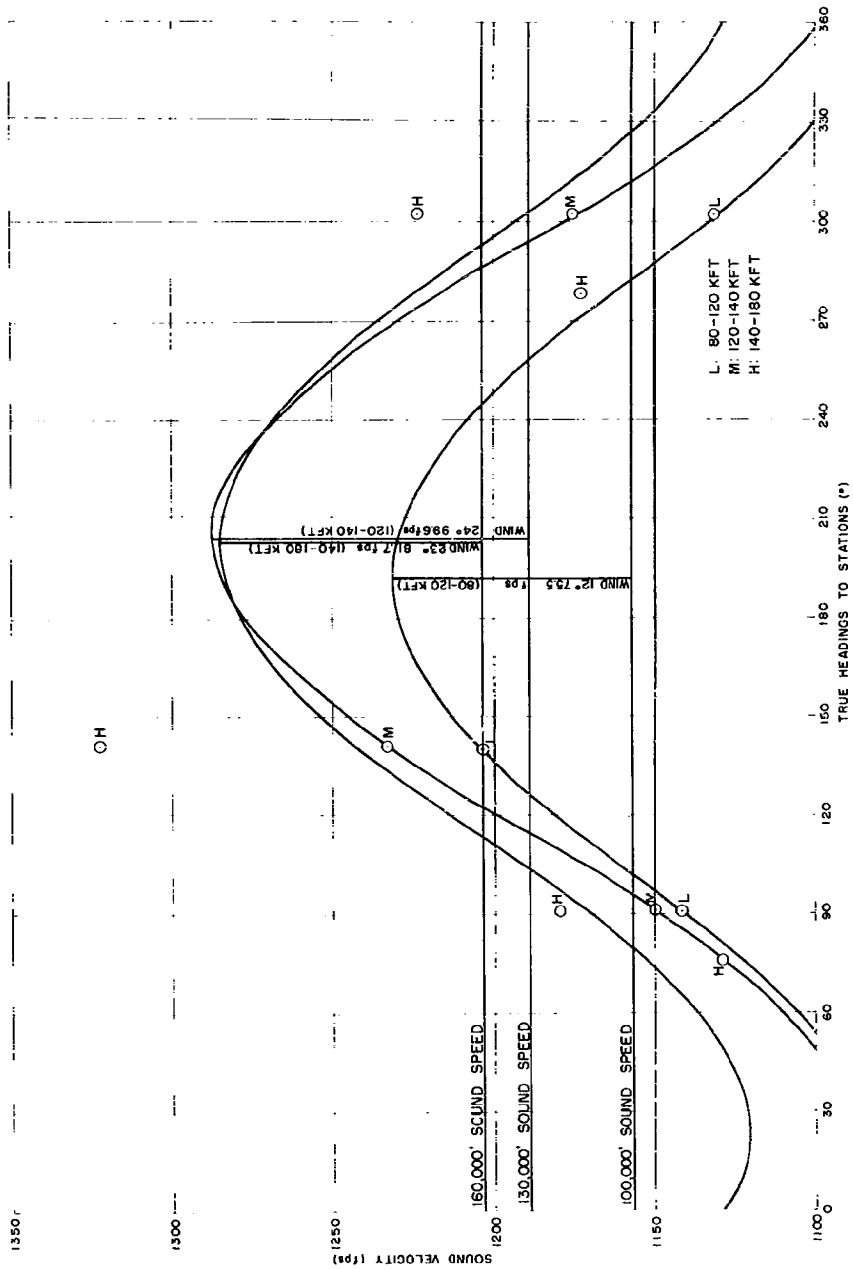

Fig. 5.9 -- Resolution of Mean Sound Velocities to Wind and Temperature Means, Upshot-Knothole

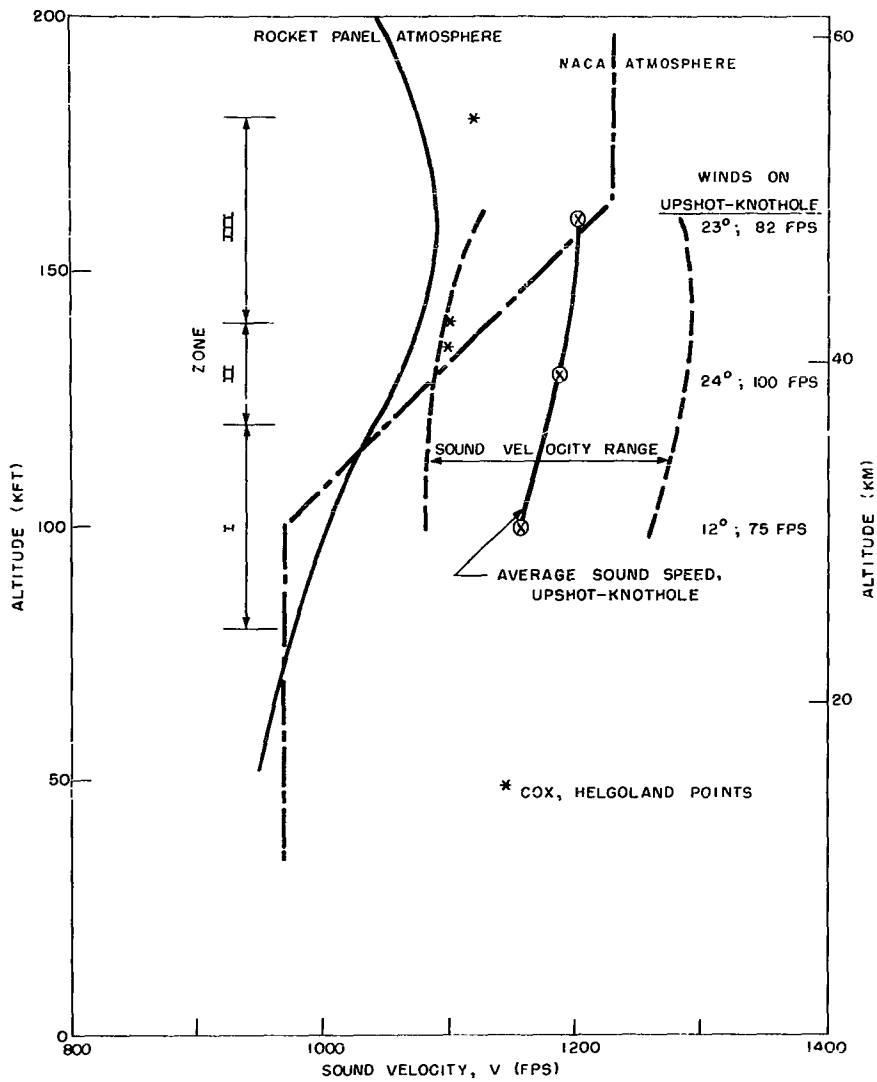

Fig. 5.10 -- Mean Ozonosphere Sound Speeds and Winds, Upshot-Knothole

exact number is needed for a confident estimate of maximum height of path. However, what appeared to be the best estimate of sound velocity-altitude data points for each Castle shot of mt range is shown in Fig. 5.11. The apparent mean for all the observations, which may be close to the mean sound speed, is very close to the mean for NTS sound ranging observations of high level conditions made during Upshot-Knothole. This causes further concern over attributing the large discrepancy between rocket observation data and data found by other methods to the difference in observing points.

A most interesting feature of records of megaton shots, shown in Fig. 5.12, is the appearance of nonacoustic waves. Dispersive gravity waves, similar to shallow water oscillations, which indicate oscillation of most of the depth of the atmosphere, are observed to arrive somewhat before ozonospheric sound signals. Sharp shocks are also observed, in Fig. 5.12, to arrive at very high incidence angles, up to 45 degrees, which, according to Eq 5.9, would have required 2000-3000 fps ambient velocities in the 300,000- to 400,000-foot region for acoustical refraction back to ground. The strength of these cracks suggests that these waves were propagated as shock waves in accordance with the Rankine Hugoniot relations rather than as sound waves, and ray tracing for shock waves to large distances requires further theoretical study for explanation.

5.4 OBSERVATIONS FROM OPERATION TEAPOT

The full benefit of experience from Upshot-Knothole and Castle was applied in operating microbarographs on Teapot. The need for exact time synchronization between stations of a pair was stressed, and precise surveys for relative spacing and orientation of the pairs were obtained. Six dual stations were operated, completely circling the test site as shown in Fig. 2.7, for confident resolution of wind and temperature components of the deduced high-altitude sound velocities.

The results of the ozonosphere observation program are listed in Table 5.1, giving winds and temperatures observed for each shot. Temperature-height curves observed during 1955 are shown in Fig. 5.13 with the Rocket Panel Atmosphere curve for reference. In Fig. 5.14, the chronological sequence of upper wind observations for the entire operation is shown. From this figure, it appears that the seasonal change from winter westerlies to summer season easterlies, reported by other observers and summarized by Gerson, [33] may be better expressed as a shift from winter northwesterlies to summer northeasterlies.

In a few instances during this operation, some uncertainty prevailed as to whether certain recorded signals had traveled one atmospheric cycle to 150,000-200,000 feet or two cycles to half that altitude. Often these signals had characteristic velocities of 1300-1600 fps

which could not very well be placed below 100,000 feet. However, with the postulated temperature-height decrease above about 160,000 feet, extremely high wind speeds would be necessary to explain these signals by acoustic refraction. When an adequate shock refraction theory has been derived, these signals may possibly be interpreted as refracted shock waves. However, some observations at a different distance along the radial to a station observing these peculiar signals would greatly aid in identifying the layer responsible for refracting these sounds to earth.

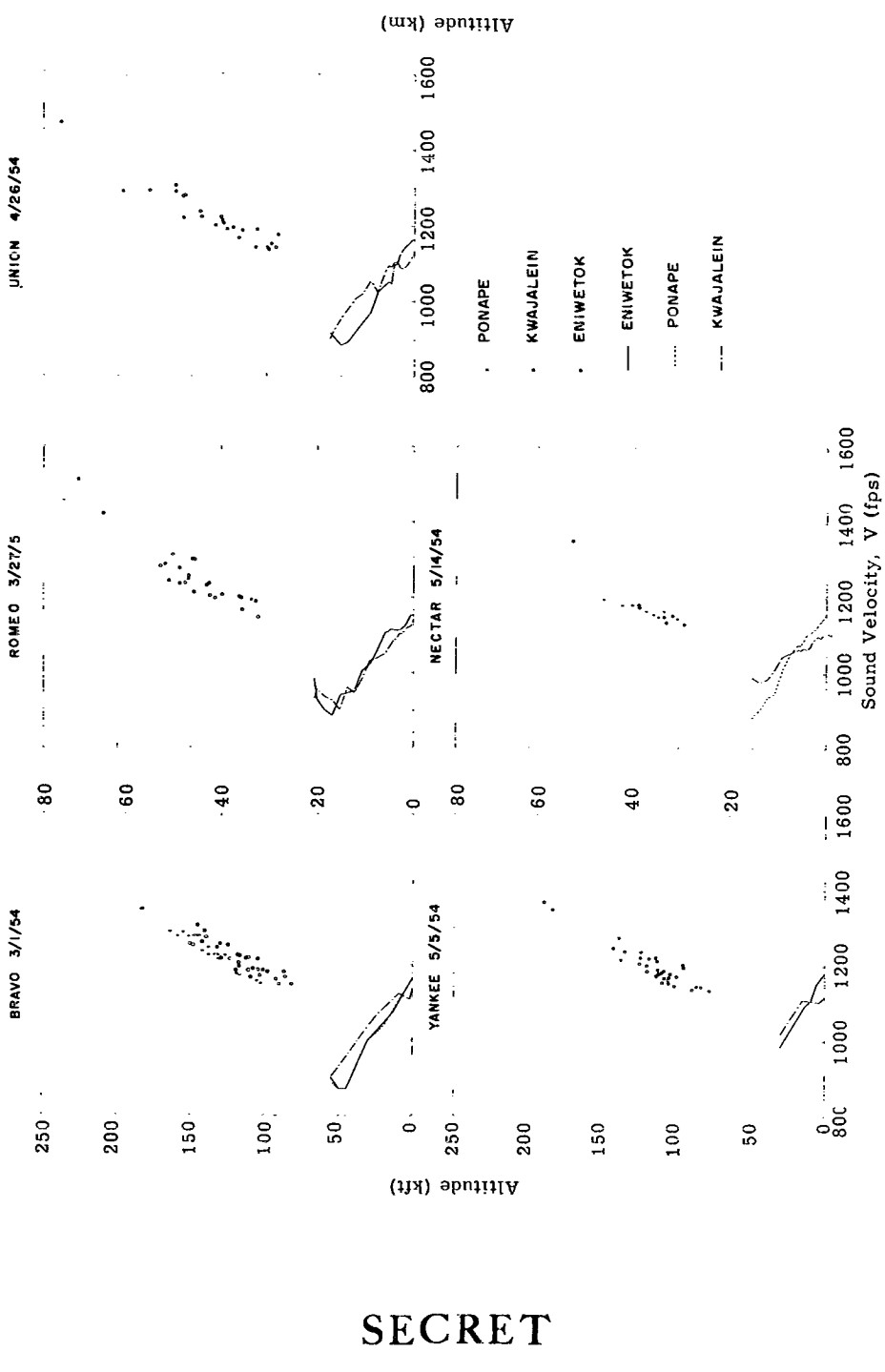

Fig. 5.11 -- Observed Upper Air Sound Velocities, Castle

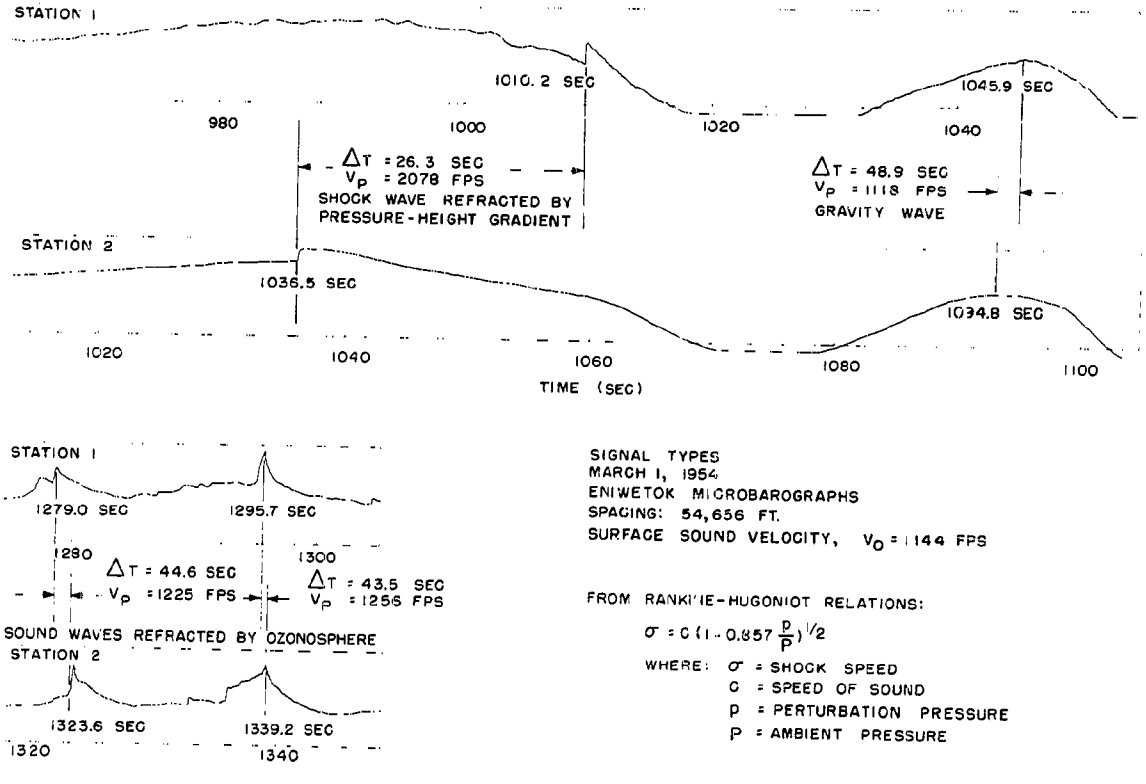

Fig. 5.12 -- Sound Signal Recording, Bravo Shot, Castle

TABLE 5.1

Ozonosphere Observation Program Results

Alt (ft, MSL)	Wind (fps)	Sound Speed (fps)	Temp (^{o}C)	Number of Stations
	Moth Summary 2/22/55, 0545 PST			
100,000	339^{o}/62	1058.5	-14.6	5
110,000	336^{o}/56	1091.8	+1.9	5
120,000	326^{o}/48	1115.0	+13.7	5
130,000	334^{o}/58	1137.6	+25.4	6
140,000	332^{o}/60	1161.7	+38.2	6
150,000	328^{o}/59	1182.9	+48.5	6
160,000	321^{o}/58	1208.8	+62.7	6
170,000	310^{o}/58	1218.5	+68.2	6
180,000	309^{o}/77	1232.1	+75.8	4
	Hornet Summary 3/12/55, 0520 PST			
70,000	277^{o}/29	1023.32	-22.4	5 (+1 extrap)
80,000	034^{o}/42	1092.49	+1.2	5
90,000	033^{o}/36	1100.88	+5.5	6
100,000	004^{o}/25	1102.48	+6.3	4
110,000	009^{o}/28	1120.87	+15.7	4
120,000	010^{o}/24	1132.36	+21.6	4
130,000	010^{o}/25	1148.61	+30.2	4
140,000	013^{o}/39	1161.77	+37.1	4
	Turk Summary 3/7/55, 0520 PST			
100,000	323^{o}/46	1064.45	-12.6	6
110,000	008^{o}/20	1108.61	+9.4	6
120,000	359^{o}/14	1120.00	+15.2	5
130,000	323^{o}/21	1128.96	+19.9	5
140,000	308^{o}/38	1133.58	+22.3	4
150,000	296^{o}/48	1143.85	+27.6	4
160,000	324^{o}/64	1152.95	+32.4	4
	Wasp Summary 2/18/55, 1200 PST			
100,000	013^{o}/64	1073.1	-7.5	4
110,000	007^{o}/67	1096.0	+4.0	4
120,000	346^{o}/62	1110.0	+11.1	4
130,000	334^{o}/76	1127.4	+20.1	3

TABLE 5.1 (cont)

Alt (ft, MSL)	Wind (fps)	Sound Speed (fps)	Temp (^{O}C)	Number of Stations
		Dee Summary 3/22/55, 0505 PST		
90,000	008^{O}/31	1091.6	+0.8	5
100,000	357^{O}/28	1099.7	+4.9	5
110,000	009^{O}/39	1122.3	+16.4	4
120,000	001^{O}/39	1136.0	+23.5	4
130,000	344^{O}/37	1150.3	+31.0	4
140,000	334^{O}/43	1177.5	+45.6	3
150,000	323^{O}/43	1197.2	+56.4	3
		Ess Summary 3/23/55, 1230 PST		
100,000	006^{O}/33	[illegible]	[illegible]	[illegible]
110,000	041^{O}/41	1134.7	+22.8	5
120,000	039^{O}/39	1151.8	+31.9	4
130,000	027^{O}/32	1166.[illegible]	+39.[illegible]	4
140,000	010^{O}/29	1180.[illegible]	+47.2	4
150,000	060^{O}/16	1202.[illegible]	+58.2	4
		Tesla Summary 3/1/55, 0530 PST		
100,000	290^{O}/54	1049.8	-19.8	4
110,000	287^{O}/31	1096.4	+3.2	4
120,000	303^{O}/20	1130.8	+20.8	4
130,000	288^{O}/30	1144.3	+27.9	4
140,000	274^{O}/40	1158.8	+35.5	4
150,000	254^{O}/72	1161.0	+36.7	3
		Apple Summary 3/29/55, 0455 PST		
90,000	028^{O}/20	1099.4	+4.7	6
100,000	060^{O}/21	1119.9	+15.2	6
110,000	052^{O}/32	1137.7	+24.4	5
120,000	043^{O}/47	1159.9	+36.2	5
130,000	036^{O}/18	1161.5	+37.0	4
140,000	032^{O}/27	1184.2	+49.3	4
150,000	027^{O}/32	1198.6	+57.1	4

TABLE 5.1 (cont)

Alt (ft, MSL)	Wind (fps)	Sound Speed (fps)	Temp (°C)	Number of Stations
		Wasp' Summary 3/29/55, 1000 PST		
100,000	035°/18	1117.7	+14.1	6
110,000	052°/29	1139.4	+25.3	5
120,000	347°/15	1143.8	+27.6	3
130,000	343°/12	1159.3	+35.8	3
140,000	325°/12	1174.7	+44.1	4
150,000	300°/21	1183.8	+49.0	4
		Post Summary 4/9/55, 0430 PST		
80,000	071°/46	1068.5	-12.7	6
90,000	065°/40	1086.9	-1.5	..
100,000	050°/30	1097.5	+3.8	5
110,000	036°/26	1111.8	+11.0	5
120,000	037°/45	1138.3	+24.1	4
130,000	039°/51	1163.9	+38.3	4
140,000	038°/53	1188.2	+51.4	4
150,000	030°/86	1234.4	+77.1	3
		Met Summary 4/15/55, 1115 PST		
90,000	021°/46	1107.8	+10.0	6
100,000	026°/45	1129.1	+21.0	5
110,000	353°/38	1133.3	+23.2	4
120,000	340°/45	1146.3	+30.0	4
130,000	351°/57	1175.8	+45.8	5
		Apple II Summary 5/5/55, 0510 PDST		
90,000	106°/33	1086.8	-0.6	6
100,000	107°/16	1100.9	+6.5	6
110,000	016°/4	1116.9	+14.7	6
120,000	137°/3	1123.7	+18.2	6
130,000	143°/13	1127.3	+20.0	6
140,000	133°/11	1136.1	+24.6	6
150,000	060°/4	1136.2	+24.7	5
160,000	071°/10	1142.2	+27.8	5
170,000	073°/19	1149.5	+31.7	5

TABLE 5.1 (cont)

Alt (ft, MSL)	Wind (fps)	Sound Speed (fps)	Temp (^{o}C)	Number of Stations
	Zucchini Summary 5/15/55, 0500 PDST			
70,000	061^{o}/55	1044.3	-21.5	5
80,000	053^{o}/56	1069.0	-9.5	5
90,000	043^{o}/60	1097.0	+4.5	5
100,000	039^{o}/68	1124.9	+18.8	5
110,000	043^{o}/90	1142.1	+27.8	4
120,000	037^{o}/62	1141.6	+27.5	3
130,000	032^{o}/58	1148.5	+31.2	3

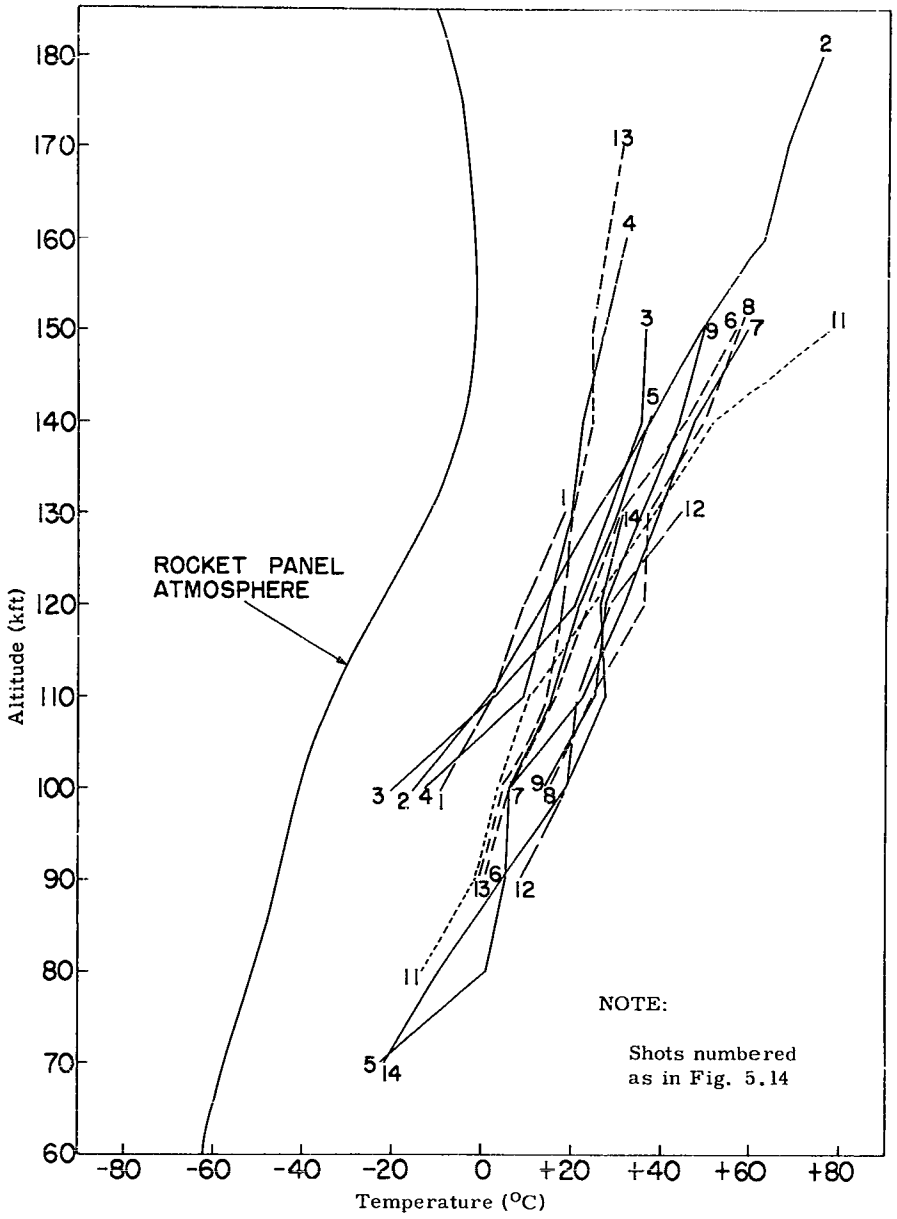

Fig. 5.13 -- Ozonosphere Temperatures Observed During Teapot

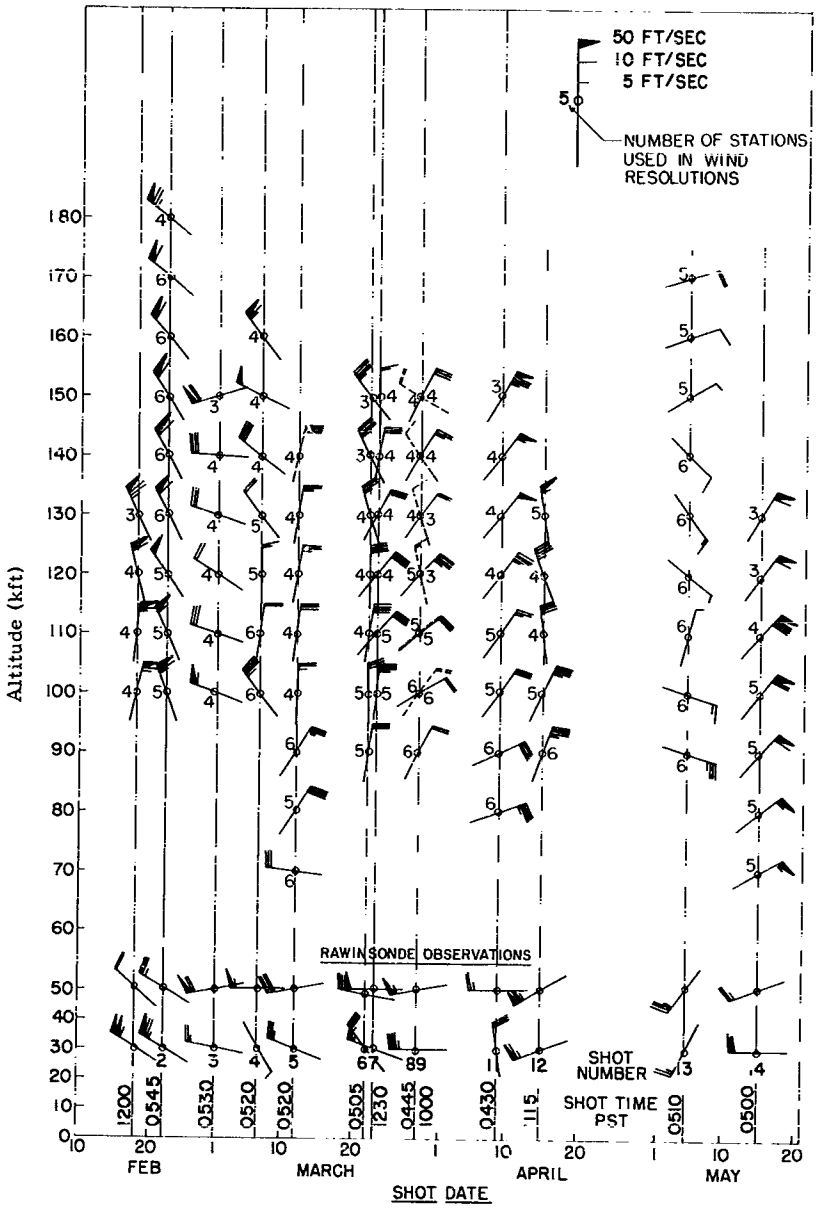

Fig. 5.14 -- Ozonosphere Winds Observed During Teapot

CHAPTER 6

RECOMMENDATIONS FOR FUTURE OPERATIONS

An attempt should be made to observe overpressure-distance gradients near focal point ranges. This could probably be done with reasonable success by four recording stations operating near and just beyond Indian Springs for one or two special HE shots at times of strong complex atmospheric ducts. Although these conditions would not be suitable for nuclear testing, a temporary station change could be made without losing nuclear test data.

Microbarograph recording systems should be re-engineered to develop a more portable and reliable instrument. Today, greatly improved stable amplifier systems are available which could be used to reduce package size, decrease maintenance time and skill requirements, and reduce operator qualification levels.

With a simplified measurement system, remote location recorders should be operated by local contract personnel at considerable financial and manpower saving. If very stable equipment is developed, remote-controlled operation could even be considered.

Further development of a reliable zero-time indicator should be supported.

An attempt should be made to derive a simplified method for ray-path calculations for low-energy shock propagation at very low ambient pressures to explain certain signals recorded both in the Pacific and in Nevada.

The program for observing ozonosphere weather conditions from sound propagation should be continued, at least until adequate rocket sounding techniques and capabilities have been demonstrated. In particular, these observations should be made during the International Geophysical Year (IGY) 1956-1958. Statements of at least moral support from other agencies interested in high-altitude research are solicited to help justify this continued program.

A system for rapidly reducing ozonosphere signal data should be developed so that wind and temperature observations could be made available on a synoptic basis.

The Raypac computer should be modified so that input data on winds and temperatures may be programmed to the computer as received from the weather station.

High-explosive preliminary shots could be eliminated with only a small measure of risk that conditions existing in the ozonosphere would refract damaging signals into St. George,

Las Vegas, and Boulder City. For predicting signals propagated through lower layers, Raypac computations are more economical and provide equal or superior verifications than scaling from HE detonations.

To reduce uncertainties in prediction for the test site area, further study of relatively short range propagation (to 0.1 psi) under inversions should be made. It was difficult to convince test operations personnel of the fact that the prediction unit verified much better at a range of 100 miles than of 10 miles. Also, the light structural damages due to a tactical shot made under an inversion should be made more predictable.

CHAPTER 7

SUMMARY

Microbarographic observation and blast prediction systems used during Operations Upshot-Knothole, Castle, and Teapot were reasonably successful. During this 2-year period, techniques were introduced which allowed rapid prediction of possible damaging blast propagation to large distances, with adequate accuracy which was largely limited by the uncertainties of predicting the weather. No serious incidents of long-range physical damage occurred, unfavorable public reactions were confined to irritations caused by audible noises.

A method has been derived for observing ozonosphere signals so that conditions of temperature and wind in the ozonosphere may be deduced with reasonable confidence and a limited number of calculations. Unless adequate and accurate rocket-borne sounding techniques are attained, the method appears to be, at present, the most feasible and economical for obtaining data on this region of the atmosphere for the IGY.

Planning and development is under way for continuing the program, at least through foreseeable test operations.

REFERENCES

1. Cox, E. F., Plagge, H. J., and Reed, J. W., Damaging Air Shocks at Large Distances from Explosions, Operation BUSTER-JANGLE, WT-303, April 24, 1952 (SRD).
2. Cox, E. F., Air Shocks at Large Distances from Atomic Explosions, Operation TUMBLER-SNAPPER, WT-504, January 5, 1953 (SRD).
3. Cox, E. F., Plagge, H. J., and Reed, J. W., "Meteorology Directs Where Blast Will Strike," Bull Am Met Soc 35 (3) 95 (March 1954).
4. "Departures of Monthly Average Temperatures from Normal, Map Chart," Monthly Weather Review 81 (5) May 1953.
5. Blast Damage Summary, Private Communication from General Adjustment Bureau, Inc., San Francisco, California, to Las Vegas Field Office, AEC, no date (Unc).
6. Church, P. K., Sandia Diaphragm-Type Pressure Transducer for Shock Wave Measurements, Sandia Corporation, SC-3305(TR), January 6, 1954 (Unc).
7. Durham, H. B., Raypac—A Special Purpose Analog Computer, Sandia Corporation TM-46-55-54, March 24, 1955 (Unc).
8. Microbarograph Evaluation Report, Sandia Corporation, SC-2990(TR), September 18, 1953.
9. Reed, J. W., et al, Ground-Level Microbarographic Pressure Measurements from a High-Altitude Shot, Operation TEAPOT, WT-1103, December 1955 (SRD).
10. Sander, H. H., Automatic Zero-Time Mark for Microbarograph Records, Sandia Corporation, TM-146-55-51, May 10, 1955 (Confidential).
11. Thompson, R. H., On Instrumentation and Operation of the Microbarograph Stations, Sandia Corporation, TM-245-54-52, January 5, 1955 (Confidential).
12. DuMond, J. W. M., et al, "A Determination of the Wave Forms and Laws of Propagation and Dissipation of Ballistic Shock Waves," J. Acoust. Soc. of Amer. 18, No. 1, p. 97, July 1946.
13. Kirkwood, J. G., and Brinkley, S. R., Jr., Theory of the Propagation of Shock Waves from Explosive Source in Air and Water, OSRD 4814 (1945).
14. Curtiss, W., Free Air Blast Measurement on Spherical Pentolite, Ballistic Research Research Laboratory Memorandum Report 544 (1951).
15. Cox, E. F., "Sound Propagation in Air," Encyclopedia of Physics (Handbuch der Physik), Springer-Verlag: Berlin, Vol. 48, Ch 22, 1957.
16. Cowan, M., Negative-Phase Duration as a Measure of Blast Yield, Sandia Corporation, SC-3170(TR), September 1, 1953 (SRD).
17. Bethe, Hans A., (ed), Blast Wave, Vol. VII, Part II, Chapter 7, Los Alamos Scientific Laboratory, LA-1021, August 13, 1947 (SRD).
18. IBM Problem M (performed at Los Alamos Scientific Laboratory), original data tabulations.
19. Letter, Cox, E. F., to Distribution, Ref. Sym: 5110(132), Subj: "Predicting Blast Pressures in Las Vegas," November 20, 1953.
20. Morgan, Lt. Col. D. N., and Wyatt, Lt. Col. W. H., Air Weather Service Participation, Operation UPSHOT-KNOTHOLE, WT-703, July 1953 (Confidential
21. Reed, J. W., "The Representativeness of Winds Aloft Observations," Bull Am Met Soc 35 (6) 253 (June 1954).
22. Operational Research into the Detailed Structure of the Jet Stream, U. S. Navy Bureau of Aeronautics Technical Report No. 1 of Project AROWA, Task 15, nd.

REFERENCES (cont)

23. Johnson, C. T., et al, Experimental Study of Explosion-Generated Acoustic Waves Propagated in the Atmosphere, U. S. Naval Electronics Laboratory Report 290, May 1, 1952.
24. Crary, A. P., "Stratosphere Winds and Temperatures from Acoustical Propagation Studies," J Meteor Vol. 7, No. 3, 1950.
25. Crary, A. P., "Stratosphere Winds and Temperatures in Low Latitudes from Acoustical Propagation Studies," J Meteor Vol. 9, No. 2, 1952.
26. Crary, A. P., and Bushnell, V. C., "Determination of High Altitude Winds and Temperatures in the Rocky Mountain Area by Acoustic Soundings, October 1951" J Met Vol. 12, No. 5, October 1955.
27. Cox, E. F., et al, "Upper-Atmosphere Temperatures from Helgoland Big Bang," J Meteor, Vol. 6, No. 5, 1949.
28. Berndes, A. E., Jr., et al, Propagation of Acoustic Waves in Air to a Distance of 300 Miles, Final report of AFOAT-1 Project Authorization B/10/A/ONR/NEL, February 15, 1954 (Confidential).
29. Kennedy, W. B., and Brogan, L., Determination of Atmospheric Winds and Temperature in the 30-60 Km Region by Acoustic Means, Denver Research Institute Final Report on Contract AF 19(122)-252, June 30, 1954.
30. Kennedy, W. B., et al, "Further Acoustical Studies of Atmospheric Winds and Temperatures at Elevations of 30 to 60 Milometers," J Met, Vol. 12, No. 6, December 1955.
31. The Rocket Panel, "Pressures, Densities, and Temperatures in the Upper Atmosphere," Phys Rev 88 (5), December 1952.
32. Warfield, C. N., "Tentative Tables for the Properties of the Upper Atmosphere," National Advisory Committee for Aeronautics Technical Note 1200, January 1947.
33. Gerson, N. C., "Seasonal Variations in Wind Velocity," Proceedings of Conference on Motions in the Upper Atmosphere, Albuquerque, New Mexico, September 7-9, 1953, National Science Foundation.

DISTRIBUTION

Military Distribution Category 5-21

ARMY ACTIVITIES

1 Asst. Dep. Chief of Staff for Military Operations, D/A, Washington 25, D.C. ATTN: Asst. Executive (R&SW)
2 Chief of Research and Development, D/A, Washington 25, D.C. ATTN: Atomic Division
3 Chief of Ordnance, D/A, Washington 25, D.C. ATTN: ORDTX-AR
4 Chief Signal Officer, D/A, P&O Division, Washington 25, D.C. ATTN: SIGRD-8
5 The Surgeon General, D/A, Washington 25, D.C. ATTN: Chief, R&D Division
6- 7 Chief Chemical Officer, D/A, Washington 25, D.C.
8 The Quartermaster General, D/A, Washington 25, D.C. ATTN: Research and Development
9- 12 Chief of Engineers, D/A, Washington 25, D.C. ATTN: ENGNB
13 Chief of Transportation, Military Planning and Intelligence Div., Washington 25, D.C.
14- 16 Commanding General, Headquarters, U. S. Continental Army Command, Ft. Monroe, Va.
17 President, Board #1, Headquarters, Continental Army Command, Ft. Sill, Okla.
18 President, Board #2, Headquarters, Continental Army Command, Ft. Knox, Ky.
19 President, Board #3, Headquarters, Continental Army Command, Ft. Benning, Ga.
20 President, Board #4, Headquarters, Continental Army Command, Ft. Bliss, Tex.
21 Commanding General, U.S. Army Caribbean, Ft. Amador, C.Z. ATTN: Cal. Off.
22- 23 Commanding General, U.S. Army Europe, APO 403, New York, N.Y. ATTN: OPOT Div., Combat Dev. Br.
24- 25 Commandant, Command and General Staff College, Ft. Leavenworth, Kan. ATTN: ATIS(AS)
26 Commandant, The Artillery and Guided Missile School, Ft. Sill, Okla.
27 Secretary, The U. S. Army Air Defense School, Ft. Bliss, Texas. ATTN: Maj. Gregg D. Brellegan, Dept. of Tactics and Combined Arms
28 Commanding General, Army Medical Service School, Brooke Army Medical Center, Ft. Sam Houston, Tex.
29 Director, Special Weapons Development Office, Headquarters, CONARC, Ft. Bliss, Tex. ATTN: Capt. T. E. Skinner
30 Commandant, Walter Reed Army Institute of Research, Walter Reed Army Medical Center, Washington 25, D. C.
31 Superintendent, U.S. Military Academy, West Point, N. Y. ATTN: Prof. of Ordnance
32 Commandant, Chemical Corps School, Chemical Corps Training Command, Ft. McClellan, Ala.
33 Commanding General, Research and Engineering Command, Army Chemical Center, Md. ATTN: Deputy for RW and Non-Toxic Material
34- 35 Commanding General, Aberdeen Proving Grounds, Md. ATTN: Director, Ballistics Research Laboratory
36 Commanding General, The Engineer Center, Ft. Belvoir, Va. ATTN: Asst. Commandant, Engineer School
37 Commanding Officer, Engineer Research and Development Laboratory, Ft. Belvoir, Va. ATTN: Chief, Technical Intelligence Branch
38 Commanding Officer, Picatinny Arsenal, Dover, N.J. ATTN: SPSR-CK
39 Commanding Officer, Army Medical Research Laboratory, Ft. Knox, Ky.
40- 41 Commanding Officer, Chemical Corps Chemical and Radiological Laboratory, Army Chemical Center, Md. ATTN: Tech. Library
42 Commanding Officer, Transportation R&D Station, Ft. Eustis, Va.
43 Director, Technical Documents Center, Evans Signal Laboratory, Belmar, N.J.
44 Director, Waterways Experiment Station, P0 Box 631, Vicksburg, Miss. ATTN: Library
45 Director, Armed Forces Institute of Pathology, Walter Reed Army Medical Center, 6825 16th Street, N.W., Washington 25, D.C.
46 Director, Operations Research Office, Johns Hopkins University, 7100 Connecticut Ave., Chevy Chase, Md. Washington 15, D.C.
47- 48 Commanding General, Quartermaster Research and Development, Command, Quartermaster Research and Development Center, Natick, Mass. ATTN: CBR Liaison Officer
49 Commanding Officer, Diamond Ordnance Fuze Laboratories, Washington 25, D. C.
50- 54 Technical Information Service Extension, Oak Ridge, Tenn.

NAVY ACTIVITIES

55- 56 Chief of Naval Operations, D/N, Washington 25, D. C. ATTN: OP-36
57 Chief of Naval Operations, D/N, Washington 25, D.C. ATTN: OP-03EG
58 Director of Naval Intelligence, D/N, Washington 25, D.C. ATTN: OP-922V
59 Chief, Bureau of Medicine and Surgery, D/N, Washington 25, D.C. ATTN: Special Weapons Defense Div.
60 Chief, Bureau of Ordnance, D/N, Washington 25, D.C.
Chief of Naval Personnel, D/N, Washington 25, D.C.
61 Chief, Bureau of Ships, D/N, Washington 25, D.C. ATTN: Code 348
62 Chief, Bureau of Yards and Docks, D/N, Washington 25, D.C. ATTN: D-440
63 Chief, Bureau of Supplies and Accounts, D/N, Washington 25, D.C.
64- 65 Chief, Bureau of Aeronautics, D/N, Washington 25, D.C.
66 Chief of Naval Research, Department of the Navy Washington 25, D.C. ATTN: Code 811
67 Commander-in-Chief, U.S. Pacific Fleet, Fleet Post Office, San Francisco, Calif.
68 Commander-in-Chief, U.S. Atlantic Fleet, U.S. Naval Base, Norfolk 11, Va.
69- 72 Commandant, U.S. Marine Corps, Washington 25, D.C. ATTN: Code AO3E
73 President, U.S. Naval War College, Newport, R.I.
74 Superintendent, U.S. Naval Postgraduate School, Monterey, Calif.
75 Commanding Officer, U.S. Naval Schools Command, U.S. Naval Station, Treasure Island, San Francisco, Calif.
76 Commanding Officer, U.S. Fleet Training Center, Naval Base, Norfolk 11, Va. ATTN: Special Weapons School
77- 78 Commanding Officer, U.S. Fleet Training Center, Naval Station, San Diego 36, Calif. ATTN: (SWP School)
79 Commanding Officer, Air Development Squadron 5, VX-5, U.S. Naval Air Station, Moffett Field, Calif.
80 Commanding Officer, U.S. Naval Damage Control Training Center, Naval Base, Philadelphia, Pa. ATTN: ABC Defense Course
81 Commander, U.S. Naval Ordnance Laboratory, Silver Spring 19, Md. ATTN: EE
82 Commander, U.S. Naval Ordnance Laboratory, Silver Spring 19, Md. ATTN: EH
83 Commander, U.S. Naval Ordnance Laboratory, Silver Spring 19, Md. ATTN: R
84 Commander, U.S. Naval Ordnance Test Station, Inyokern, China Lake, Calif.

85 Officer-in-Charge, U.S. Naval Civil Engineering Res. and Evaluation Lab., U.S. Naval Construction Battalion Center, Port Hueneme, Calif. ATTN: Code 753
86 Commanding Officer, U.S. Naval Medical Research Inst., National Naval Medical Center, Bethesda 14, Md.
87 Director, Naval Air Experimental Station, Air Material Center, U.S. Naval Base, Philadelphia, Penn.
88- 92 Chief, Bureau of Aeronautics, D/N, Washington 25, D.C. ATTN: AER-AD-41/20
93 Director, U.S. Naval Research Laboratory, Washington 25, D.C. ATTN: Mrs. Katherine H. Cass
94 Commanding Officer and Director, U.S. Navy Electronics Laboratory, San Diego 52, Calif.
95- 96 Commanding Officer, U.S. Naval Radiological Defense Laboratory, San Francisco, Calif. ATTN: Technical Information Division
97- 98 Commanding Officer and Director, David W. Taylor Model Basin, Washington 7, D.C. ATTN: Library
99 Commander, U.S. Naval Air Development Center, Johnsville, Pa.
100 CINCPAC, Pearl Harbor, TH
101 Commander, Norfolk Naval Shipyard, Portsmouth 8, Va. ATTN: Code 270
102-106 Technical Information Service Extension, Oak Ridge, Tenn. (Surplus)

AIR FORCE ACTIVITIES

107 Asst. for Atomic Energy Headquarters, USAF, Washington 25, D.C. ATTN: DCS/O
108 Director of Operations, Headquarters, USAF, Washington 25, D.C. ATTN: Operations Analysis
109 Director of Plans, Headquarters, USAF, Washington 25, D.C. ATTN: War Plans Div.
110 Director of Research and Development, DCS/D, Headquarters, USAF, Washington 25, D.C. ATTN: Combat Components Div.
111-112 Director of Intelligence, Headquarters, USAF, Washington 25, D.C. ATTN: AFOIN-1B2
113 The Surgeon General, Headquarters, USAF, Washington 25, D.C. ATTN: Bio. Def. Br., Pre. Med. Div.
114 Asst. Chief of Staff, Intelligence, Headquarters, U.S. Air Forces-Europe, APO 633, New York, N.Y. ATTN: Directorate of Air Targets
115 Commander, 497th Reconnaissance Technical Squadron (Augmentcd), APO 633, New York, N.Y.
116 Commander, Far East Air Forces, APO 925, San Francisco, Calif. ATTN: Special Asst. for Damage Control
117 Commander-in-Chief, Strategic Air Command, Offutt Air Force Base, Omaha, Nebraska. ATTN: Special Weapons Branch, Inspector Div., Inspector General
118 Commander, Tactical Air Command, Langley AFB, Va. ATTN: Documents Security Branch
119 Commander, Air Defense Command, Ent AFB, Colo.
120-121 Research Directorate, Headquarters, Air Force Special Weapons Center, Kirtland Air Force Base, New Mexico, ATTN: Blast Effects Res.
181-185 Technical Information Service Extension, Oak Ridge, Tenn. (Surplus)

ATOMIC ENERGY COMMISSION ACTIVITIES

186-188 U.S. Atomic Energy Commission, Classified Technical Library, 1901 Constitution Ave., Washington 25, D.C ATTN: Mrs. J. M. O'Leary (For DMA)
189-193 Los Alamos Scientific Laboratory, Report Library, PO Box 1663, Los Alamos, N. Mex. ATTN: Helen Redman
194-198 Sandia Corporation, Classified Document Division, Sandia Base, Albuquerque, N. Mex. ATTN: H. J. Smyth, Jr.
199-201 University of California Radiation Laboratory, PO Box 808, Livermore, Calif. ATTN: Clovis G. Craig
202 Weapon Data Section, Technical Information Service Extension, Oak Ridge, Tenn.
203-215 Technical Information Service Extension, Oak Ridge, Tenn. (Surplus)
122 Commander, Air Research and Development Command, PO Box 1395, Baltimore, Md. ATTN: RDDN
123 Commander, Air Proving Ground Command, Eglin AFB, Fla. ATTN: Adj./Tech. Report Branch
124-125 Director, Air University Library, Maxwell AFB, Ala.
126-133 Commander, Flying Training Air Force, Waco, Tex. ATTN: Director of Observer Training
134 Commander, Crew Training Air Force, Randolph Field, Tex. ATTN: [illegible], DCS/O
135-136 Commandant, Air Force School of Aviation Medicine, Randolph AFB, Tex.
137-142 Commander, Wright Air Development Center, Wright-Patterson AFB, Dayton, O. ATTN: WCOSI
143-144 Commander, Air Force Cambridge Research Center, LG Hanscom Field, Bedford, Mass. ATTN: CRQST-2
145-147 Commander, Air Force Special Weapons Center, Kirtland AFB, N. Mex. ATTN: Library
148 Commander, Lowry AFB, Denver, Colo. ATTN: Department of Special Weapons Training
149 Commander, 1009th Special Weapons Squadron, Headquarters, USAF, Washington 25, D.C.
150-151 The RAND Corporation, 1700 Main Street, Santa Monica, Calif. ATTN: Nuclear Energy Division
152 Commander, Second Air Force, Barksdale AFB, Louisiana. ATTN: Operations Analysis Office
153 Commander, Eighth Air Force, Westover AFB, Mass. ATTN: Operations Analysis Office
154 Commander, Fifteenth Air Force, March AFB, Calif. ATTN: Operations Analysis Office
155 Commander, Western Development Div. (ARDC), PO Box 262, Inglewood, Calif. ATTN: WDSIT, Mr. R. G. Weitz
156-160 Technical Information Service Extension, Oak Ridge, Tenn. (Surplus)

OTHER DEPARTMENT OF DEFENSE ACTIVITIES

161 Asst. Secretary of Defense, Research and Development, D/D, Washington 25, D.C. ATTN: Tech. Library
162 U.S. Documents Officer, Office of the U.S. National Military Representative, SHAPE, APO 55, New York, N.Y.
163 Director, Weapons Systems Evaluation Group, OSD, Rm 2E1006, Pentagon, Washington 25, D.C.
164 Armed Services Explosives Safety Board, D/D, Building T-7, Gravelly Point, Washington 25, D.C.
165 Commandant, Armed Forces Staff College, Norfolk 11, Va. ATTN: Secretary
166 Commander, Field Command, Armed Forces Special Weapons Project, PO Box 5100, Albuquerque, N. Mex.
167 Commander, Field Command, Armed Forces Special Weapons Project, PO Box 5100, Albuquerque, N. Mex. ATTN: Technical Training Group
168-169 Commander, Field Command, Armed Forces Special Weapons Project, P.O. Box 5100, Albuquerque, N. Mex. ATTN: Deputy Chief of Staff, Weapons Effects Test
170-180 Chief, Armed Forces Special Weapons Project, Washington 25, D.C. ATTN: Documents Library Branch

Defense Special Weapons Agency
6801 Telegraph Road
Alexandria, Virginia 22310-3398

TRC

24 June 1998

MEMORANDUM TO DEFENSE TECHNICAL INFORMATION CENTER
ATTENTION: OCQ/Mr. William Bush

SUBJECT: Declassification of AD-342207 ~~S-RD~~

The Defense Special Weapons Agency Security Office has reviewed and declassified the following document:

AD-342207
WT-9003
General Report on Weapons Tests, Long-Distance Blast Predictions, Microbarometric Measurements, and Upper-Atmosphere Meteorological Observations For Operations Upshot-Knothole, Castle, and Teapot, by E. F. Cox and J. W. Reed, Sandia Corporation, Albuquerque, New Mexico, Issuance Date: September 29, 1957.

Distribution statement **"A"** (approved for public release) now applies.

Ardith Jarrett
ARDITH JARRETT
Chief, Technical Resource Center

Completed
B.W
1-24-2000